PLANETARY ROVER MOBILITY ON LOOSE SOIL: TERRAMECHANICS THEORY FOR SIDE SLIP PREDICTION AND COMPENSATION

NICOLÒ CARLETTI

Supervisor: Prof. Michéle Lavagna

Master of Science
Space Engineering
Department of Aerospace Science and Technology

Politecnico di Milano

December 2016 – 816663

ABSTRACT

The aim of this thesis is to develop a model which can predict a mobile trajectory profile of the rover under loose soil condition. The study also encapsulates a traversal run in a sloped terrain without the skid characteristics.
The geometry and features are defined to model the rover as known as Moonraker: the lunar rover of the team HAKUTO, competing for the Google Lunar XPRIZE.
After a brief introduction of the working environment, a chapter is dedicated to the modeling of the forces generated from the interaction between wheels with soil, depending on the slip ratio and the slip angle. The used model is the one proposed by G. Ishigami [6, 7, 8, 9], based on the work of M. G. Bekker [1, 2] and J. Y. Wong [3] and modified, according to what proposed by M. Sutoh [11, 12, 13], to explicitly consider the grouser effect. The model is verified through *One-Wheel* tests.
The equations of motion are retrieved and the numerical simulation with iterative loop is described.
The desired state is reached imposing arbitrary inputs to the wheels. Two input strategies are discussed: torque input and velocity input.
The resulting motion is compared with tests on both controlled (sandbox) and uncontrolled environment. The former is mainly used to verify the precision of the model, and the latter to prove the sensibility to the ground properties.
The independence of the model from the traveling velocity is verified, employing the same tests used for the main goal of the thesis.
The aim of the thesis is reached defining the strategy for the compensation of the side slip on a slope terrain. A tuning procedure is performed to correct the model errors and fit the desired system performances. The initial attitude of the rover is studied in order to compensate the drifting angle with a proper orientation. A "slope-attitude" correlation is defined interpolating the found solutions. The validity of the obtained solution is tested and verified.

SOMMARIO

Lo scopo di questa tesi è realizzare un modello che sia in grado di predire la traiettoria di un rover che si muove su terreno sabbioso. Lo studio comprende inoltre un possibile approccio per la correzione dello slittamento laterale, presente durante l'attraversamento di un pendio.
La geometria e le caratteristiche del sistema in analisi sono definite al fine di descrivere il robot noto come Moonraker: il rover lunare del team HAKUTO, il quale compete per il Google Lunar XPRIZE.
Dopo una breve introduzione sull'argomento trattato, un capitolo è dedicato all'analisi e descrizione del modello di forze generate dalla interazione tra le ruote e il suolo, in relazione alla variazione di rateo di slittamento e angolo di slittamento (rispettivamente *slip ratio* e *slip angle* in inglese). Il modello che viene utilizzato è quello proposto da G. Ishigami [6, 7, 8, 9], il quale si basa sul lavoro di M. G. Bekker [1, 2] e J. Y. Wong [3]. A questo viene aggiunto il contributo di forze dovuto alle sporgenze presenti sulle ruote (in inglese *grousers*), secondo quanto proposto da M. Sutoh [11, 12, 13]. Il modello risultante viene quindi verificato, comparandolo con quanto ottenuto da test eseguiti su una ruota dotata di sensori di forza e momento.
Avendo illustrato il sistema studiato con le opportune approssimazioni, sono presentate le equazioni del moto e la simulazione numerica, necessarie per l'elaborazione della traiettoria.
Il raggiungimento dello stato desiderato per la simulazione è garantito da un input agente sulle ruote: *in primis* viene descritto come si possa usare il momento generato dai motori per controllare la dinamica delle ruote, e in seguito viene illustrato come imporre direttamente la velocità di rotazione sia più congeniale al problema.
Il moto risultante dalle simulazioni è confrontato con quanto ottenuto in test svolti in un ambiente controllato (*sandbox*) e naturale. Lo scopo dei primi è quello di permettere un confronto, ben conoscendo le variabili presenti. I test svolti nel secondo ambiente servono ad evidenziare come la conoscenza di questi parametri sia fondamentale per una buona simulazione. Attraverso gli stessi test usati per gli obiettivi principali della tesi, è accennato uno studio atto a dimostrare come la velocità di manovra non influenzi il percorso, non modificando le forze presenti.
Lo scopo della tesi è raggiunto con il confronto del modello proposto con quanto ottenuto durante questi test. A questo segue una proposta di regolazione dei parametri al fine di minimizzare l'errore di simulazione. Avendo il modello ottimizzato, è possibile studiare un opportuno angolo con cui affrontare il pendio, il quale garantisca un moto

orizzontale. Iterando questo procedimento per tutte le pendenze in esame, è possibile definire una curva che relazioni l'inclinazione del suolo con l'orientazione da assumere al fine di attraversare il percorso. La soluzione proposta viene quindi verificata con ulteriori test, per dimostrarne l'efficacia.

Alla mia famiglia.

CONTENTS

LIST OF FIGURES

LIST OF TABLES

1 INTRODUCTION

> The Earth is the cradle of humanity, but mankind cannot stay in the cradle forever.
>
> Konstantin Tsiolkovsky

1.1 HISTORICAL BACKGROUND

Since the beginning of the modern rocketry, thanks to the work of Konstantin Tsiolkovsky, the humankind started to look at the celestial bodies with the eager to conquer them, knowing that the technology was ready to push them that far.
The Soviet Union managed in the October 1957 to send the first artificial satellite on orbit around the Earth, the Sputnik 1: this event signed the beginning of a new era in the space exploration. United States and Soviet Union, willing to prove the country supremacy and power, invested a great amount of money in this field, granting a tremendous advancing in the related technology. During January 1959, The Soviet Union firstly succeeds in performing a Moon fly-by with the Luna 1 mission. Other missions followed, culminating with the Luna 3, that managed to send for the first time images of the dark side of the Moon. Another record was reached by the Soviet Union when on the 12th of April, 1961, Yuri Gagarin became the first man to reach the space on the Vostok 1. In the following eight years, sixty-nine American and U.S.S.R. missions gave us a better understanding of the Moon, Venus and Mars. It was on the 16th July, 1969, that we made *a giant leap*: Neil A. Armstrong is the first man to walk on the Moon surface, during the mission Apollo 11.
The first Moon Rover was landed by the Soviet Union the following year. During the mission Luna 17, the Lunokhod 1 started its mission that lasted 322 days, traveling a distance of 10540 meters and sending to the ground station thousands of images and various ground analysis.
Many other lunar mission were successfully carried on until 1976, when the main interest became the realization of space stations and the exploration of other celestial bodies, leaving the Moon settlements missions unrealized.
Japan became the third country to orbit around our satellite in the 1990.

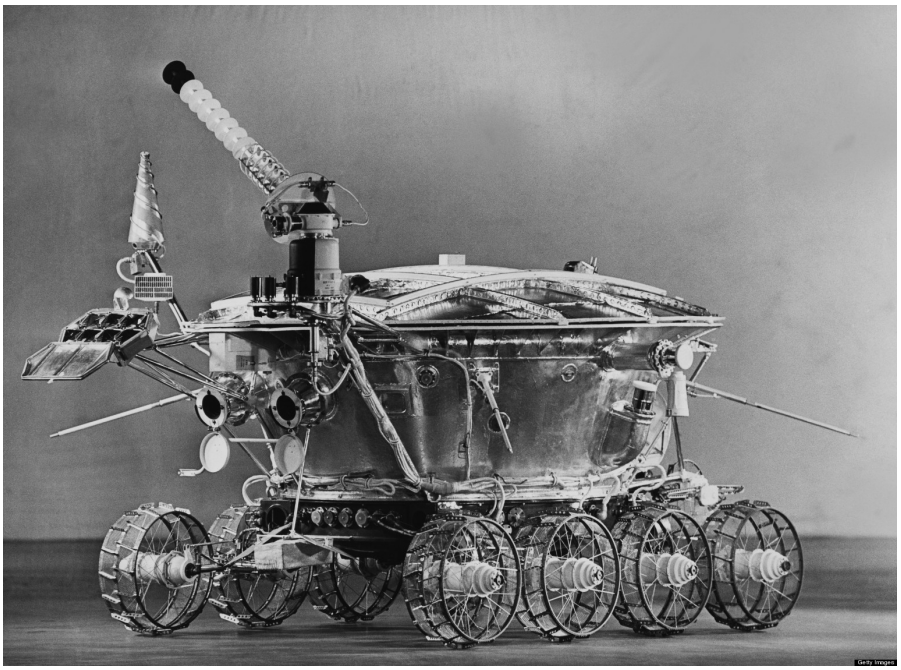

Figure 1: Lunokhod 1

In the 2000s, other countries managed to reach the Moon. Of great interest is the Indian satellite Chandrayaan-1 that, in 2008, discovered great evidence of water in the Moon soil. In 2013, China became the third country to land a rover on the Moon during the Chang'e 3 mission.
The following year, another important step has been made. To honor the death of Manfred Fuchs (OHB Systems founder), the first commercial mission to the Moon took place.

1.2 GOOGLE LUNAR XPRIZE

On September 2007, XPRIZE Foundation, along with Google inc., announced the Google Lunar XPrize.
What is the Google Lunar XPRIZE?

> The $30M Google Lunar XPRIZE (GLXP) is an unprecedented competition to challenge and inspire engineers, entrepreneurs and innovators from around the world to develop low-cost methods of robotic space exploration. To win the Google Lunar XPRIZE, a privately funded team must be the first to:
>
> - successfully place a spacecraft on the Moon's surface
> - travel 500 meters

Figure 2: Google Lunar XPrize logo

- transmit high-definition video and images back to Earth

The first team that successfully completes this mission will be awarded the $20 million Grand Prize. The second team to successfully complete the mission will be awarded $5 million. To win either of these prizes, teams must prove that 90% of their mission costs were funded by private sources. Teams have until the end of 2016 to announce a verified launch contract to remain in the competition and complete their mission by the end of 2017.[33]

The aim of this competition is to revolutionize the idea that outer space is not a dream but affordable travel to anyone. The advancement is not achievable without the emergence of the private ventures by developing cutting technologies while reducing the expenses. As shown above, manned and unmanned robotic vehicle are an essential component in the exploration of any celestial body. Those low budget rovers are surely fundamental in the upcoming lunar bases project that are again being considered for the next two decades.
The Moon has been selected for this challenge for being the *closest neighbor* and so granting a perfect environment for testing and developing new technologies, useful for future space exploration. It also has a lot of elements that are rare on Earth (China is willing to mine the Moon in order to retrieve the Helium-3) and the presence of water makes it of great interests for many researches.
The competition expects the team to finish the mission by the end of

December 2017. The team still competing for the prizes are counting at 16 (over 34). Three of them (SpaceIL, Moon Express and Synergy Moon) have secured a verified launch contract (with SpaceX, Rocket Lab and Interorbital Systems respectively). The others have time until the end of 2016 to ensure one. Team HAKUTO is partnered with an American team, Astrobotic, and its rover will fly on Astrobotic's lander Griffin. To make the challenge more interesting for the competitors, other achievements grant smaller amount of money: those are all connected to technology improvements such as traveling far distances, finding evidence of ice or recording images and videos of the landing site of one of the Apollo Program landing sites or any man-made item. Remarkable is the additional million is granted to teams that make significantly promote ethnic diversity in STEM (Science, Technology, Engineering and Mathematics) fields, underlining the main purpose of the challenge.
On January 2015, 5 teams were awarded with prizes ranging from 500.000 dollars to 1.75 million dollars (HAKUTO, Part-Time Scientists, Team Indus, Moon Express and Astrobotic respectively).

1.3 HAKUTO

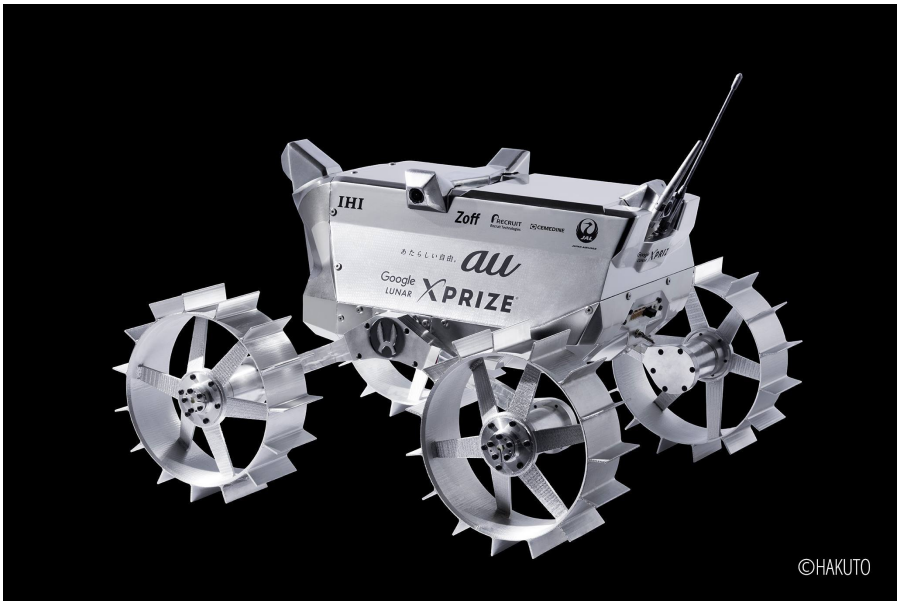

Figure 3: HAKUTO PFM3 Moonraker

Team HAKUTO, whos leader is Takeshi Hakamada, is the only japanese GLXP team. The team is under the operation of ispace inc., a Tokyo-based space company created to provide space-related marketing, media opportunities and engineering services. The team is partnered with the Space Robotics Lab (SRL), led by Professor Yos-

hida in the Department of Aerospace and Mechanical Engineering at Tohoku University, Sendai.
XPRIZE Foundation announced the Terrestrial Milestone Prize (TMP) in October of 2013: a cash prizes of $250 thousand USD to $1 million USD to five eligible teams in mobility, landing and imaging categories in order to speed up the development. In January 2015, HAKUTO was awarded $500 thousand USD for a successful testing campaign including radiation, thermal vacuum [17], vibration and field testing.

1.3.1 *Moonraker*

The design concept for the Moonraker (Figure 3) was to keep it as light as possible, in order to satisfly the strict constrains of the mission, while not sacrificing mobility performance over lunar regolith, especially on steep slopes of 20° or more that may be encountered in the predicted path. The design led to a total weight of 8 kg. Actuation points were kept minimal, reducing mass and failure modes. The key design features are large relative wheel size and 4 cameras, to have a 360° coverage. There's a TOF laser ragefinder in the front of the rover for detecting obstacles that the cameras might fail to. A 4 wheel configuration has been preferred over the 6 one because enables to have the wheel diameter doubled, occupying the same volume (enhancing the slip control performances). The slippage reduction is also enhanced by the presence of grousers. The wheels were therefore designed to be 20 cm in diameter with 2.25 cm grousers. Laboratory experiments indicate that a slip ratio of under 0.1 should be expected with these wheels on slopes of up to 10°. According to the design philosophy, no steering mechanism is present. Two kind of maneuvering are considered: spot turn, rotating the left and right wheels with the same velocity of opposite direction, and skid steering, where the wheels rotate in the same direction, with different velocities. The traveled distance is measured as average of the wheels rotation, as measured by the motors encoders.

1.3.2 *Tetris*

The Space Robotics Lab has also developed a small, 2 kg child rover, called Tetris, that, together with Moonraker, composes a dual rover system. Tetris will be tethered to Moonraker, which will serve as an anchor for exploration into pits and down steep cliffs.

1.4 PURPOSE AND APPROACH

Because of the loose soil, locomotion on the Moon is a challenging mission by itself. The loose soil causes a certain slippage on the wheel, that leads to an erroneous evaluation of the position, if not properly considered.
The purpose of this thesis is to provide a tool to predict the dynamics of a rover, with determined features, operating on flat or inclined terrain, in presence of loose soil.
To do that it is necessary to develop:

- an analytical model for the *wheel-soil* interaction
- a model of the rover dynamics on loose soil

Develop an analytical model for the *wheel-soil* interaction

The first purpose of this work is to analyze and model the interaction between rigid wheels and loose soil. The discipline that studies this field is called Terramechanics. For planet exploration, being able to predict correctly the dynamics of the rover is crucial: if models for rigid ground are applied, an erroneous evaluation of distances is obtained, being the slippage not considered. The slip is due to a difference between the wheel velocity and the vehicle velocity. This can be dangerous for two reasons, linked to two aspect of the slip. The longitudinal slip causes problems in the evaluation of the precise traveled distance. For long distances this can lead to a misevaluation of the position. If too high, the longitudinal slip can also make the wheel dig and correspondingly get stuck in the sand. The side slip (or skid) is related to the later movement experienced in the slopes. Due to the presence of cliffs and caves, not being able to predict and control the side slip can result in the failure of the mission.
Terramechanics models are being studied since the '60s by Mieczysław G. Bekker that is considered the father of this discipline and had a significant role in the design of the rovers used in the Apollo 15, Apollo 16, Apollo 17 missions. Jo Y. Wong greatly contributed in the study of the stress generation beneath the wheels. Those models aim to determine the shape and intensity of those stresses. Doing this, it is possible to evaluate the reaction forces and torques acting on each wheel.
The obtained results are verified through tests operated on a single wheel, having a force/torques sensor (F/T sensor) mounted.

Model of the rover dynamics on loose soil

The second purpose is to model the rover dynamics, moving on loose soil. Having the geometry of the rover fixed, the equations of

motion are retrieved and, using a SIMULINK® model, the dynamics is simulated. The input to be given are the desired states of the wheel. Given that, the forces are evaluated through the above described force model, and the rover state computed. The simulated trajectories are then compared with the results of tests performed in a sandbox, using the Moonraker itself.

2 WHEEL-SOIL MODEL

In this chapter, the *wheel-soil* contact model is developed. As introduced above, the basis of this work is given by Bekker in [1, 2] and Wong in [3, 29]. A wide use of the Tohoku Uiversity research heritage has also been used. In particular the publications of G. Ishigami [6, 7, 8, 9] and M. Sutoh [11, 12, 13] are a solid background and guidelines for this thesis.
The key parameters are the relationship between *pressure-sinkage* and the slip ratio, that are used as input for the whole model. To be noticed that the velocity is not a variable and it has no effect on the resultant forces. This is verified through experiments for the commonly used velocity for rovers, that are up to 5 cm/s. The equation describing the pressure-sinkage relationship is the one proposed by Bekker-Reece. The equation approximates the stresses generated by a flat plate penetrating into the soil, and that is used to evaluate the three-axis forces and two torques generated on the wheel, later described in detail.

2.1 WHEEL REFERENCE FRAME

For this thesis, a right-handed reference frame, centered in the central axis of the wheel, is considered. The y axis is orthogonal to the wheel lateral surface, the z axis is orthogonal to the ground and the x axis is consequently pointing forward the moving direction. The reference frame rotates with the wheel if steerings occours, but it doesn't rotate with the wheel rotation.

2.2 WHEEL SINKAGE

One of the most intuitive differences between solid ground and loose soil, is that the wheels sinks in the terrain. The sinkage of the wheels is of primary importance to understand the phenomenon, since it creates the contact area between wheel and soil, that will determine the forces generated.
This sinkage is addressed to two summed effects.

$$h = h_{st} + h_{dyn} \tag{1}$$

The static sinkage (h_{st}) is due to the normal load on the wheel, the dynamic sinkage (h_{dyn}) is due to the wheel rotation.

Static sinkage

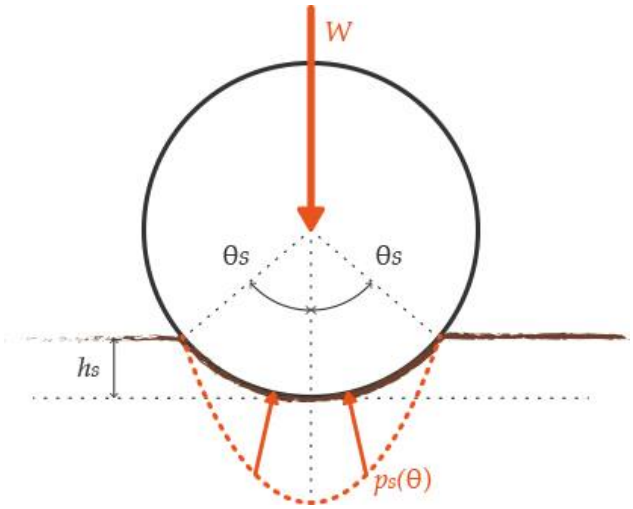

Figure 4: Static sinkage

In his work, Bekker considered a rectangular flat plate acting on homogeneous soil. The static stress generated is modeled as in (2).

$$p(h) = \left(\frac{k_c}{b} + k_\phi\right) h^n \tag{2}$$

In this equation various parameters are introduced. First of all, the static pressure (related to the sinkage h) is defined as p. b is the smaller width of the plate, k_c and k_ϕ are respectively the cohesive and frictional moduli of deformation (or pressure-sinkage moduli) and n is the deformation sinkage exponent. k_c, k_ϕ and n are experimentally obtained in the so called penetration test, from the relation pressure-sinkage of two different plates. This procedure is described in [6].
Equation (2) is modified by Reece as in (3).

$$p(h) = (ck'_c + \rho b k'_\phi)\left(\frac{h}{b}\right)^n \tag{3}$$

The parameter c is defined as the cohesion stress of soil and ρ is the wight density of the terrain.
The parameters k'_c and k'_ϕ have the same meaning in (2) and in (3), but in the first, their dimension changes depending on the value of n, while in the second those are dimensionless. To be noted that, if n is equal to 1, (2) and (3) are the same, considering $k_c = ck'_c$ and $k_\phi = \rho k'_\phi$. Equation (3) is the one used in this thesis.
An important parameter is defined as the static angle θ_s, that is the angle between the vertical with respect to the ground and the contact point of the wheel with the soil, measured in the center of the wheel. Using a geometrical approach, a simple equation correlating the wheel angle θ and the sinkage is obtained as in (4).

$$h(\theta) = r(\cos\theta - \cos\theta_s) \tag{4}$$

The parameter r is the wheel radius.
Substituting (4) into (3), the static pressure results linked to the wheel angle as shown in (5).

$$p(\theta) = (ck'_c + \rho bk'_\phi)\left(\frac{r(\cos\theta - \cos\theta_s)}{b}\right)^n \tag{5}$$

The vertical load of the wheel W is defined as the integral of the pressure on the whole contact area of the wheel with the soil. This results in the (6).

$$W = \int_{-\theta_s}^{\theta_s} p(\theta) br \cos\theta \, d\theta \tag{6}$$

The load W, the radius r and the wheel width b are known data. Equation (6) can be numerically solved to find the contact angle θ_s. Knowing this, the static sinkage is obtained with an easy utilization of (4) as shown in (7).

$$h_s(\theta) = r(\cos 0 - \cos\theta_s) = r(1 - \cos\theta_s) \tag{7}$$

Dynamic sinkage

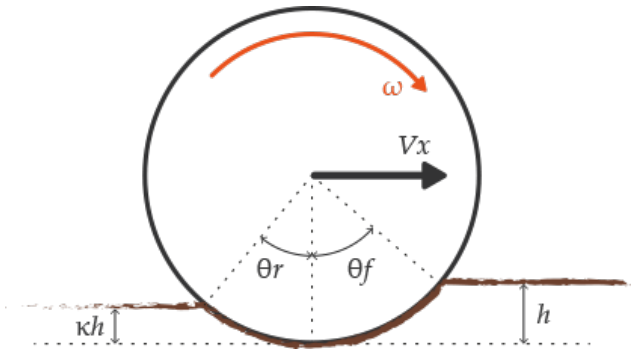

Figure 5: Wheel contact angles

The dynamic sinkage is a phenomenon that depends on a high number of parameters, depending simultaneously on the ground characteristics, wheels geometry, slip ratio simultaneously. For this reason an analytical formulation is hard to obtain. On the other hand, a numerical solution is proposed. It has already been said that the the sinkage highly influences the force generation, including the vertical reaction force as will be shown later: the higher the sinkage, the higher the forces. It is possible to evaluate the correct total sinkage, finding the value of h that satisfies $F_z(h) = W$ (F_z represents the vertical reaction force), using an iterative procedure. Once the value of h is obtained, using (1), h_{dyn} is estimated.

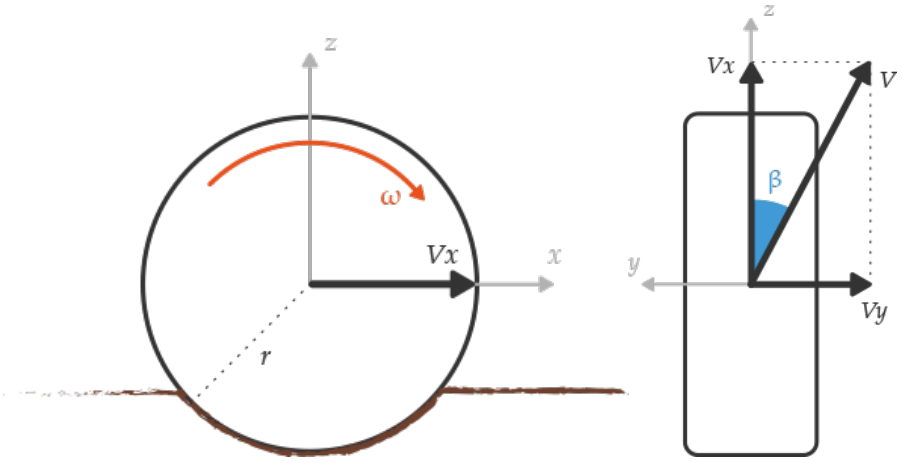

Figure 6: Wheel reference

2.3 WHEEL CONTACT ANGLE

Another effect of the wheel rotation is the variation of the contact angle from the previously evaluated static angle θ_s. Two new angles are introduced: the entry angle θ_f and the exit angle θ_r (where f stands for front and r for rear). The entry angle θ_f is defined as the angle between the vertical and the first contact point between the soil and the wheel. The exit angle θ_r is similarly defined as the angle between the vertical and the last contact point between the soil and the wheel. Those angles can be evaluated using the sinkage previously obtained. Using a geometry correlation, the θ_f is evaluated in (8).

$$\theta_f = \cos^{-1}\left(1 - \frac{h}{r}\right) \tag{8}$$

The exit angle θ_r is influenced by the rotation of the wheel and soil parameters. This is expressed with the term κ, that is the ratio between the soil height in the front and in the back of the wheel. If κ is equal to 1, it means that the sinkage is equal before and after the wheel, if higher than 1 that the soil height is higher behind the wheel and viceversa. Equation (9) describes the exit angle θ_r .

$$\theta_r = \cos^{-1}\left(1 - \frac{\kappa h}{r}\right) \tag{9}$$

2.4 SLIP RATIO

As previously introduced, when traveling on loose soil, it is common to experience some slippage. That mechanism is measured through the slip ratio s, and is defined as the ratio between the wheel angular velocity and the longitudinal velocity as expressed in (10).

$$s = \begin{cases} \frac{r\omega - v_x}{r\omega} & \text{if } |r\omega| > |v_x| \\ \frac{r\omega - v_x}{v_x} & \text{if } |r\omega| < |v_x| \end{cases} \tag{10}$$

ω is the angular velocity of the wheel, and v_x is the longitudinal velocity.
From this equations, it can be seen that the slip ratio s has values ranging between -1 and 1. The zero value represents the condition in which the velocity of the wheel is the same of the traveling velocity, and no slip occours. The first equation of the system is used when accelerating and the second one is for breaking.
The lateral component of the slip ratio is measured with the slip angle β, that is defined as the angle formed by the lateral component of the traveling velocity v_y and the longitudinal one v_x, as shown in (11).

$$\beta = \tan^{-1}\left(\frac{v_y}{v_x}\right) \tag{11}$$

2.5 STRESS MODEL

When a wheel travels on loose soil, the ground deformation generates stresses beneath the wheel, that can be modeled as normal stress σ and shear stress τ. Those stresses are responsible for the forces and torques acting on the wheel.

2.5.1 *Normal stress*

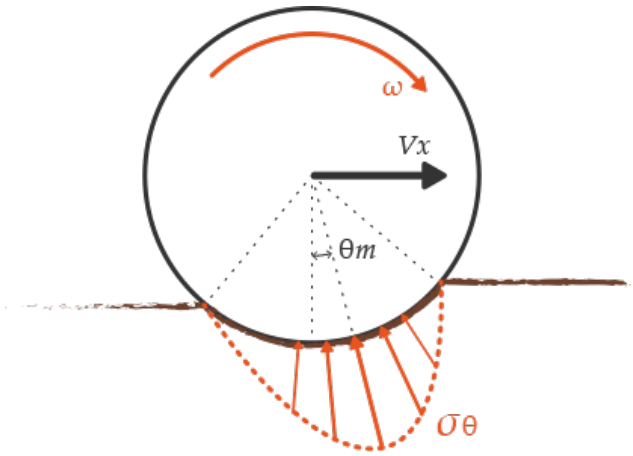

Figure 7: Normal stress

The normal stress σ is modeled based on what previously obtained with the Reece equation (3), according to what proposed in [6].

$$\sigma(\theta) = \begin{cases} (ck'_c + \rho b k'_\phi)\left(\frac{r}{b}\right)^n [\cos\theta - \cos\theta_f]^n & (\theta_m \leqslant \theta < \theta_f) \\ (ck'_c + \rho b k'_\phi)\left(\frac{r}{b}\right)^n \left[\cos\left(\theta_f - \frac{\theta-\theta_r}{\theta_m-\theta_r}(\theta_f - \theta_m)\right) - \cos\theta_f\right]^n & (\theta_r < \theta \leqslant \theta_m) \end{cases} \tag{12}$$

θ_m is the angle in which the normal stress is maximum. This point is used in the model to shape better the normal stress, changing the describing equation in that point. θ_m is experimentally obtained and described in (13).

$$\theta_m = (a_0 + a_1 s)\theta_f \tag{13}$$

a_0 and a_1 are experimental parameters that are linked to the wheel-soil interaction. They usually assume values respectively of $a_o \approx 0.4$ and $0 \leqslant a_1 \leqslant 0.3$.

2.5.2 *Shear stress*

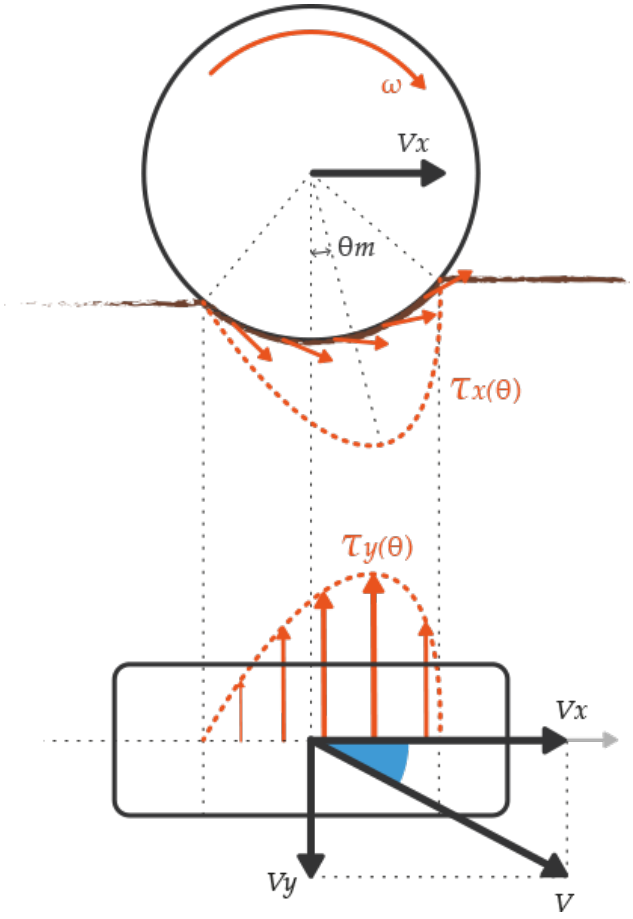

Figure 8: Shear stress

The model used is the one proposed by Janosi and Hanamoto [14]. The equation used correlates the stress with the deformation as shown in (14).

$$\begin{aligned} \tau &= \tau_{max}\left(1 - exp^{-j/\kappa}\right) \\ \tau_{max} &= c + \sigma \tan\phi \end{aligned} \tag{14}$$

τ_{max} is the maximum value that the shear stress can reach, j is a parameter related to the soil deformation and κ is the shear deformation modulus. This constant is not to be confused with the previously defined sinkage ratio. The shear deformation modulus will now on only be found as κ_x and κ_y.
c is the cohesion stress and ϕ is the internal friction angle of the soil.

Longitudinal shear stress

Since in this thesis both the longitudinal dynamic and the lateral one are analyzed, a distinction for the shear stress is highligthed, intuitively using the subscript x when referring to the longitudinal dynamics and y for the lateral dynamics. According to (14), the (15), for the longitudinal stress τ_x, is obtained.

$$\tau_x(\theta) = (c + \sigma(\theta)\tan\phi)\left(1 - e^{-j_x(\theta)/\kappa_x}\right) \tag{15}$$

As previously anticipated, the soil deformation j and the shear deformation modulus κ are expressed in term of longitudinal dynamics. The soil deformation in the x direction j_x is evaluated integrating in the time the relative velocity wheel-soil as expressed in (16), (17).

$$\begin{aligned} v_{jx}(\theta) &= r\,\omega - v_x \cos\theta \\ &= r\,\omega\left(1 - (1-s)\cos\theta\right) \end{aligned} \tag{16}$$

$$\begin{aligned} j_x &= \int_0^t v_{jx}(\theta)\,dt \\ &= \int_\theta^{\theta_f} r\,\omega\left(1 - (1-s)\cos\theta\right)\frac{1}{\omega}\,d\theta \\ &= r\left(\theta_f - \theta - (1-s)(\sin\theta_f - \sin\theta)\right) \end{aligned} \tag{17}$$

Equation (17) is consequently used in the evaluation of τ_x (15).

Lateral shear stress

Using an approach analog to what used for τ_x, the lateral shear stress τ_y is obtained in (18).

$$\tau_y(\theta) = (c + \sigma(\theta)\tan\phi)\left(1 - e^{-j_y(\theta)/\kappa_y}\right) \tag{18}$$

To express j_y, it has to be considered that the relative lateral velocity v_{jy} does not have any component due to the wheel rotation. Using the relation $v\ cos\ \theta = v_x$ and (10), (19) is obtained.

$$\begin{aligned} j_y &= \int_0^t v_{jy}(\theta)\,dt \\ &= \int_\theta^{\theta_f} v \sin\beta \frac{1}{\omega}\,d\theta \\ &= r\,(\theta_f - \theta)(1-s)\tan\beta \end{aligned} \tag{19}$$

Substituting (19) in (18), also τ_y is defined.

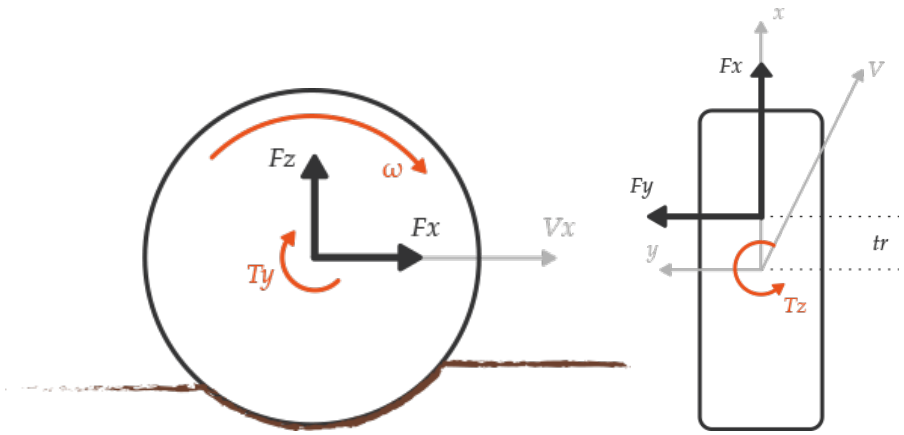

Figure 9: Wheel forces

2.6 DRAWBAR PULL

The drawbar pull F_x is the force acting in the longitudinal direction, generated by the wheel deforming the soil beneath. The drawbar pull is evaluated integrating the longitudinal stresses $\sigma(\theta)$ and $\tau_x(\theta)$ on the contact area of the wheel, delimitated by the angles θ_f and θ_r as shown in (20).

$$F_x = r\,b \int_{\theta_r}^{\theta_f} \left(\tau_x(\theta)\cos\theta - \sigma(\theta)\sin\theta\right) d\theta \tag{20}$$

2.7 SIDE FORCE

The side force F_y is generated whenever the wheel is not aligned with the movement direction or a lateral velocity is present. This force is due to two effects: the shear stress acting beneath the wheel and the soil acting on the lateral surface of the wheel itself. Therefore the side force F_y is represented as in (21).

$$F_y = F_u + F_s \sin\beta \tag{21}$$

F_u represents the lateral force generated by the lateral shear stress τ_y. F_s is the force generated by the action on the side of the wheel, that is called *bulldozing force*, called after the name of the phenomenon that generates it. The meaning of the sine is explained later on in this section.
F_u is evaluated similarly to what done with the previous forces. The lateral shear stress τ_y is integrated on the contact area as shown in (22)

$$F_u = r\,b \int_{\theta_r}^{\theta_f} \tau_y(\theta)\, d\theta \tag{22}$$

The lateral force is also due to the bulldozing phenomena. The model used to describe this phenomenon is the one proposed by Hegedus.

In this thesis only the mathematics needed for the model is presented. For a detailed analysis, [6] presents a wider review of the phenomenon.
F_s is evaluated as the integral of the bulldozing resistance $R_b(h)$, to be consistent with the usual force formulation. It is expressed in (23).

$$\begin{aligned} F_s &= \int_{\theta_r}^{\theta_f} R_b(h)\, dx \\ &= \int_{\theta_r}^{\theta_f} R_b(r - h(\theta)\cos\theta)\, d\theta \end{aligned} \tag{23}$$

the equation (24) for $R_b(h)$, is the one used in the model. It is not the general form, but it is already specialized for the wheel case.

$$R_b(h) = \left(\cot X_c + \tan(X_c + \phi)\right)\left(hc + \frac{1}{2}\rho h^2\left(\cot X_c + \frac{\cot^2 X_c}{\cot\phi}\right)\right) \tag{24}$$

ρ is the soil density and X_c is the destructive angle, a geometrical parameter obtained through experiments. Its value is related to the friction angle ϕ as shown in (25).

$$X_c = 45° - \frac{\phi}{2} \tag{25}$$

To be noted that the direction of the bulldozing force F_s is parallel to the motion of the wheel. If a steering angle β is present, the effect of the force will not be aligned with the later force F_u. For this reason, the components of F_s are to be summed to both the longitudinal and lateral forces as shown in (26).

$$\begin{aligned} F_x &= F_x^{old} - F_s\cos\beta \\ F_y &= F_u + F_s\sin\beta \end{aligned} \tag{26}$$

F_x^{old} is the longitudinal force evaluated in (20).

2.8 VERTICAL FORCE

The vertical force F_z is generated, just like the longitudinal force, by the longitudinal shear stress and mainly by the normal stress, as shown in (27).

$$F_z = rb\int_{\theta_r}^{\theta_f} \left(\tau_x(\theta)\sin\theta + \sigma(\theta)\cos\theta\right) d\theta \tag{27}$$

As mentioned in Section 2.2, the computation of the vertical force is used to find the correct sinkage. It can be clearly seen in (27), considering that all the terms are related to the sinkage itself.

2.9 RESISTANCE TORQUE

Having all the previous evaluated forces applied in the center of the wheel, also the torques must be considered. The so called resistance torque acts around the y axis and is originated by the longitudinal shear stress τ_x. For this reason it can be found in the literature as T_x. In this thesis it has been chosen, instead, to use T_y, considering it easier and more instinctive, referring to the axis around which it acts. The resistance torque T_y is expressed in (28).

$$T_y = r^2 b \int_{\theta_r}^{\theta_f} \tau_x(\theta)\, d\theta \tag{28}$$

2.10 SELF ALIGNING TORQUE

The self aligning torque T_z takes its name by the effect it has on pneumatic vehicles, that have been studied widely in the terramechanics. As already mentioned, the lateral force can be generated by a slip angle β different from zero. Due to their deformation capability, the zero moment point of the wheel is in the rear half of the wheel. Due to that, the torque T_z generated acts to reduce the angle β, realigning the wheel with the motion direction. In the case of the rigid wheel, as it is in this case, the zero moment point is in the front half of the wheel, therefore generating a torque that tends to increase the slip angle β.
Taking into consideration the definition θ_m, it is assumed that the force is applied in that point. Knowing that, the moment arm and the torque are evaluated in (29).

$$\begin{aligned} t_r &= r \sin\theta_m \\ T_z &= t_r \times T_y \\ &= r \sin\theta_m \times T_y \end{aligned} \tag{29}$$

2.11 GROUSERS

2.11.1 *Forces evaluation*

In the model since now proposed, the forces generated by the wheel are evaluated considering flat surfaces and cylindrical wheels. However it is of common knowledge that the grousers are of wide use in space exploration rovers, as many of the operating rovers do. Sutoh [11] conducted a detailed analysis on this subject and it is incorporated in the model presented in this work.
The grousers are used to enhance the grip and mobility on loose soil and rough terrain. The main result is to significantly increase the drawbar pull and vertical force and modify the slip ratio. The increased

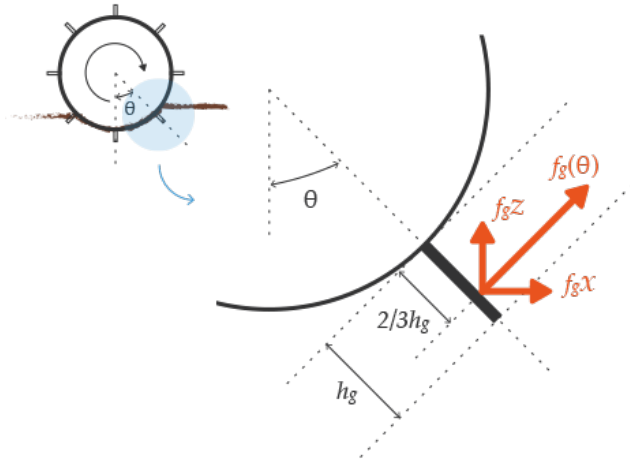

Figure 10: Grouser effect

drawbar pull also increases the resisting moment. The force and moment components due to the grousers are respectively called F_{xg} and T_{yg}. The model presented is referred specifically to the Moonraker case, where the grousers are flat and radially positioned.
The effect of the grousers is studied as a blade moving through the soil. The general equation for the pressure $\sigma_b(z)$ generated by the blade is modeled as in (30), where z is the depth of the blade in the soil.

$$\sigma_b(z) = \rho_b \, g \, z \, N_\rho + q \, N_q + c \, N_c \tag{30}$$

ρ_b is the soil bulk density, g is the gravitational constant and q is the surcharge pressure vertically acting on the soil surface. When considering the wheel case, the surcharge pressure is the normal stress σ. N_ρ, N_q and N_c are expressed as in the system (31).

$$\begin{aligned} N_\rho &= \frac{1}{2} \frac{\cot\alpha + \cot X_c}{\cos\alpha + \sin\alpha \, \cot(X_c + \phi)} \\ N_q &= 2 \, N_\rho \\ N_c &= \frac{1 + \cot X_c \, \cot(X_c + \phi)}{\cos\alpha + \sin\alpha \, \cot(X_c + \phi)} \end{aligned} \tag{31}$$

α is the angle between the grouser and the tangential of the wheel surface. X_c is equal to 45° - ϕ.
For the specific case of the grousers radially applied (α = 90°), the (30) becomes as in (32).

$$\begin{aligned} \sigma_g &= s\left(\rho \, g \, z \, N_\phi + q \, N_\phi + 2 \, c \, \sqrt{N_\phi}\right) \\ N_\phi &= \tan^2(X_c + \phi) \end{aligned} \tag{32}$$

To be noted that in the wheel case, X_c does not have a fixed value, but it has to be evaluated for each time step as the angle between the slip line and the tangential to the grouser tip. The slip ratio s is used

to take into consideration also the case when there is some slippage. Integrating the pressure σ_g on the grouser surface, the force acting at a general angle θ is obtained as in (33).

$$\begin{aligned} f_g(\theta) &= b \int_0^{h_g} \sigma_g(z)\, dz \\ &= s\, b \left(\frac{1}{2} \rho\, g\, h_g^2\, N_\phi + q(\theta)\, h_g\, N_\phi + 2\, c\, h_g \sqrt{N_\phi} \right) \end{aligned} \tag{33}$$

The effect of the grousers is not continuous, nor constant in time. Knowing that the computational effort that this model requires is significant and since the dynamics of the single grouser is not considered of big interest, it is computed the average contribute of each force generated, of the whole set of grousers, for a single rotation.
Before doing this, two geometrical parameters are introduced. α is defined as the angle between the entry and exit angles, for the non-grousered wheel (34).

$$\alpha = \theta_f - \theta_r \tag{34}$$

β is defined as the angle between two grousers (35).

$$\beta = \frac{2\pi}{N} \tag{35}$$

N is the number of grousers.
It is now possible to evaluate the force generated, that is divided according to the reference frame, in its vertical longitudinal components, and the torque generated. It is assumed a triangular shaped pressure, and so the force is applied at two third of the grouser length of distance from the wheel surface.
The result is shown in the system (36).

If $\beta > \alpha$

$$\begin{aligned} F_{xg} &= \frac{N}{2\pi} \int_{\theta_r}^{\theta_f} f_g(\theta) \cos\theta\, d\theta \\ F_{yg} &= \frac{N}{2\pi} \int_{\theta_r}^{\theta_f} f_g(\theta) \sin\theta\, d\theta \\ F_{xg} &= \left(r + \frac{2}{3} h_g \right) \frac{N}{2\pi} \int_{\theta_r}^{\theta_f} f_g(\theta)\, d\theta \end{aligned} \tag{36}$$

If $\beta < \alpha$

$$\begin{aligned} F_{xg} &= \frac{N}{2\pi} \int_{\theta_m - \beta/2}^{\theta_m + \beta/2} f_g(\theta) \cos\theta\, d\theta \\ F_{yg} &= \frac{N}{2\pi} \int_{\theta_m - \beta/2}^{\theta_m + \beta/2} f_g(\theta) \sin\theta\, d\theta \\ F_{xg} &= \left(r + \frac{2}{3} h_g \right) \frac{N}{2\pi} \int_{\theta_m - \beta/2}^{\theta_m + \beta/2} f_g(\theta)\, d\theta \end{aligned}$$

The contributes evaluated are to be summed to the forces already evaluated in (26) and (28).

2.11.2 *Slip ratio modification*

The presence of the grousers changes the diameter and shape of the wheel, making it not possible to be implemented with the previous computation. In the case under analysis, the number of grousers is high enough, in order not to have the wheel touching the ground if considered on rigid terrain (the procedure to verify this is now presented). Thanks to this, it is possible to define an ideal traveling distance, considering the shape of the wheel as a N faced polygon. The distance between two grousers tip l_t is geometrically derived as in (37).

$$l_t = (r + h_g) \sin \frac{\pi}{N} \tag{37}$$

l_u is the distance between the touching wheel and the touching grouser, in the case in which few grousers are present, and so also the wheel itself touches the hard terrain.

$$l_u = \sqrt{\left(\frac{r + h_g}{2}\right)^2 - r^2} \tag{38}$$

If l_t is smalled than l_u, the polygon approximation con be applied, and the virtual perimeter d_d measured as (39).

$$d_d = N\, l_t \tag{39}$$

In the other case, (40) must be used, where also the wheel rotation term is present.

$$d_d = 2\, N\, l_u + 2\,(\pi - \theta_{f0}\, N) \tag{40}$$

θ_{f0} is the grouser contact angle.
Considering d the real traveling distance, the slip ratio s can now be evaluated as in (41).

$$s = 1 - \frac{d}{d_d} \tag{41}$$

2.12 SLOPE CASE

2.12.1 *Reference frames*

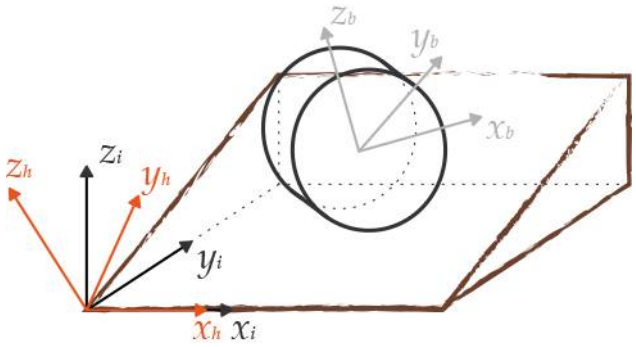

Figure 11: Reference frames

In this thesis, three reference frames are considered:

- Inertial reference frame (x_i,y_i,z_i): fixed reference frame, having the x axis aligned with the transversal direction of the slope, the z axis in the absolute vertical direction and the y axis accordingly to a right handed reference frame. Used as absolute reference.
- Horizon reference frame(x_h,y_h,z_h): reference frame obtained rotating the x inertial axis of α (slope inclination), in order to have the y axis aligned to the steepest direction and the z axis normal to the inclined surface. Reference frame used to compute the dynamics.
- Body reference frame(x_b,y_b,z_b): reference frame fixed to the principal axis of inertia of the rover. The same used in the Section 2.1 for the wheel. Used to compute the forces of the wheel-soil model.

2.12.2 *Wheel model in a sloped terrain*

In the case of a terrain, inclined of an angle α, the model can still be applied with few corrections.
The angle Φ represents the angle between x_b and the x_i-y_i plane, around the y_b axis. Φ can be evaluated as in (42).

$$\Phi = \alpha \sin\gamma \tag{42}$$

γ is the angle between x_b and x_h.
The wheel sinkage h is corrected as in (43), and attention must be put

to the normal load W, that has a component along y_h and one on z_h as in (44).

$$h_{slope} = h \cos\Phi \tag{43}$$

$$W_{slope} = W \cos\alpha \tag{44}$$

Starting from this two modified parameters, the model can be used as in the flat terrain case.

2.13 NUMERICAL SIMULATION

In this section, it is summarized the procedure to compute the interaction between the loose soil and the wheel. In the flowchart (Figure 12) presented in this section, it is suggested how to proceed with the numerical implementation of the model. For what concerns the soil parameters, there was not the possibility to perform a campaign of tests in order to obtain new results. For this reason, the values obtained by Ishigami [6] are taken as reference and reported in Table 1.
Those parameters are selected over others, because his works has

Parameter	Symbol	Value
Cohesion stress	c	0.0 kPa
Friction angle	ϕ	38.0°
Soil destructive angle	X_c	26.0°
Cohesive modulus	k'_c	0.0
Frictional modulus	k'_ϕ	120.54
Sinkage exponent	n	1.703
Maximum stress angle modulus	a_0	0.4
Maximum stress angle modulus	a_1	0.15
Soil density	ρ	$1490.0 \frac{kg}{m^3}$

Table 1: Soil parameters

been conducted in the same laboratory and with the same instrumentation used for this thesis. The soil parameters refers to the *Toyura Sand*, a common sand used for terramechanics testing. The size and shape of this sand can be easily controlled during the production, therefore creating a well known sand. More details on the tests conditions are reported in a following chapter.
The procedure is summarized as follows:

1. Set the soil parameters (c,n,k_c,k_ϕ,ϕ,ρ,κ), the wheel parameters (r,b) and the normal load W (those fixed for the whole simulation)
2. Evaluate the slip ratio s and the slip angle β
3. Determine the sinkage h with an iterative procedure, increasing the dynamic sinkage until the vertical load W is balanced by the vertical force F_z
4. Calculate the contact angles θ_f and θ_r
5. Evaluate the normal stress σ, the shear stress τ_x and τ_y
6. Calculate the resulting forces F_x, F_y, T_y,T_z

2.14 RESULTS

The proposed model is firstly analysed in its more general form, therefore without using (36), and then comparing it with how it is modified by the presence of those. The model sensibility to slip angle β and slip ratio s is highlighted.

In Figure 13, the value of the drawbar pull F_x is plotted for different values of β. The higher the value of the slip angle, the higher the intensity of the force. It is also clear how the slip ratio affects the force. The slippage induces the soil to deform more, and thus increases the stress generated. Some considerations can be done on the value of the drawbar pull when the slip ratio is null: in this condition the soil underneath the wheel cannot generate a stress that results in a positive tractive force. The value of that force, for null slip ratio, can be either null or negative.

Figure 14 shows the lateral force F_y, varying the slip ratio, and the slip angle. Its value is proportional to the slip angle β, and this explains the curve for null β.

Figure 15 and 16 show the strong relation of those torques respectively with the drawbar pull and the lateral force.

The grousers produce a force tangential to the wheel surface as shown in Figure 17. The grousers act only between the entry angle θ_f and the exit angle θ_r. As for the wheel model, if there is no slippage, no force is generated.

The grouser effect on the drawbar pull is shown in Figure 18. According to the model, the higher the number of grousers, the higher the intensity of the drawbar pull. The force intensity asymptotically reaches a value for increasing number of grousers.

When the grousers are considered, the wheel contact surface decreases. This reduction does not affect the drawbar pull, due to the grouser contribution (Figure 19), but it causes the lateral force to decrease

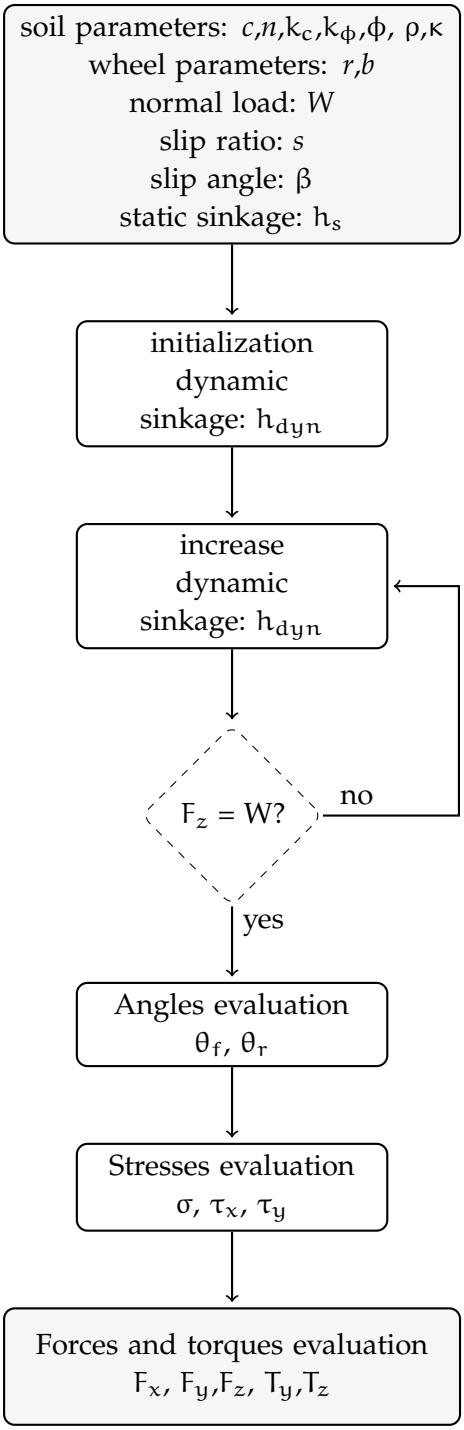

Figure 12: Numerical simulation flowchart

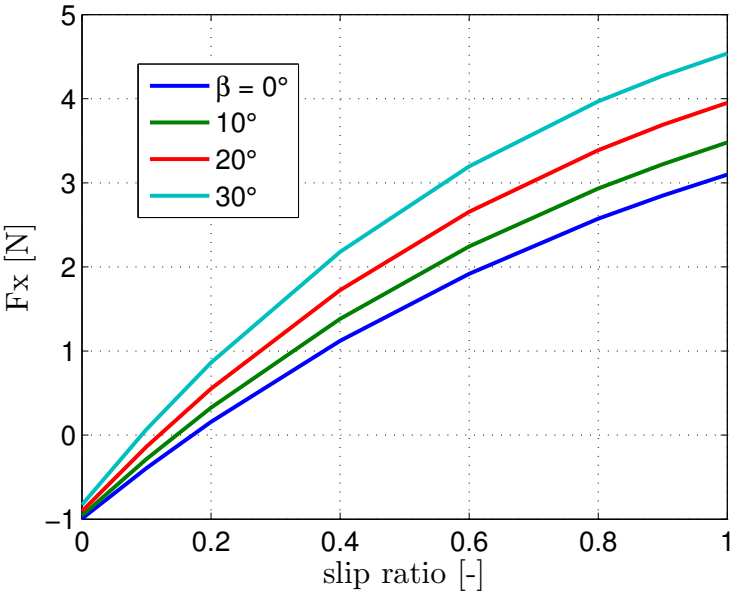

Figure 13: Fx vaying β (no grousers model)

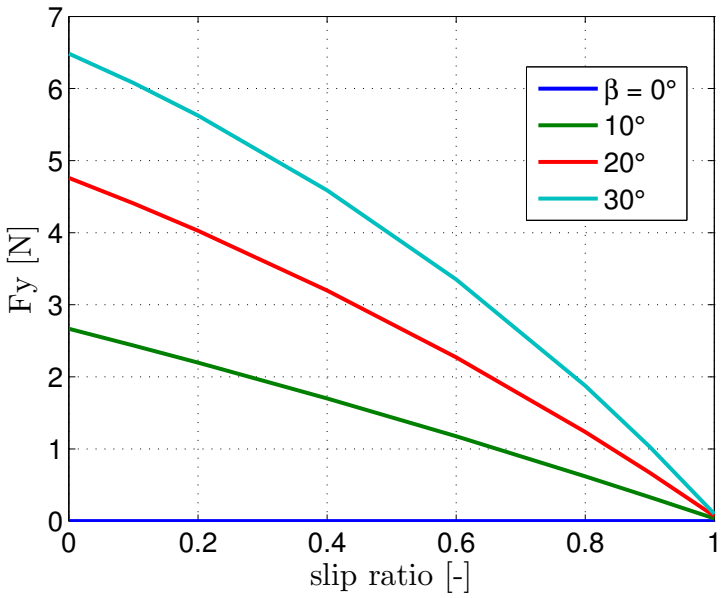

Figure 14: Fy vaying β (no grousers model)

as shown in Figure 20.

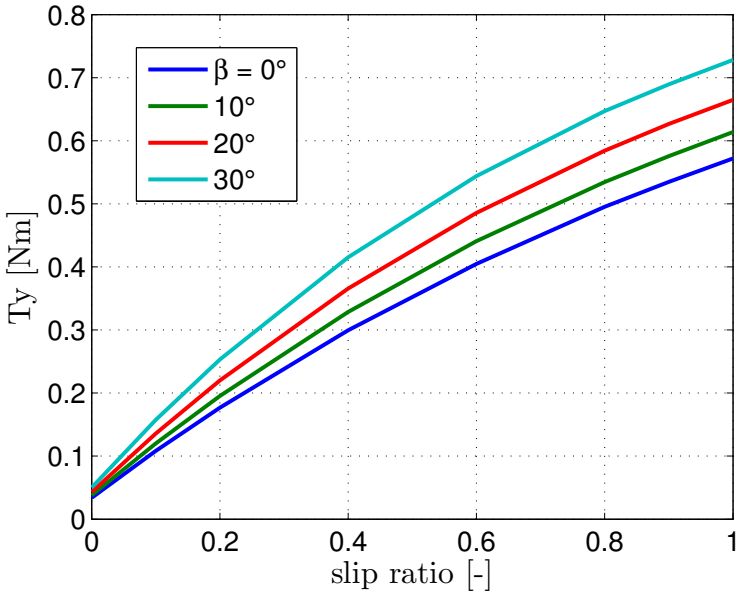

Figure 15: Tx vaying β (no grousers model)

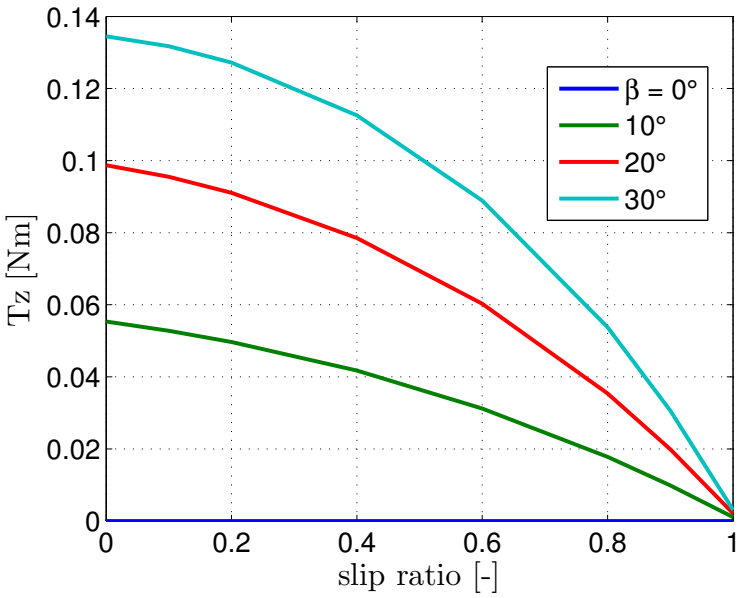

Figure 16: Tz vaying β (no grousers model)

2.15 ONE-WHEEL TEST

One-wheel testing is performed to compare the results of the Wheel-soil model with the values obtained from testing. The setup of this test is a wheel, with varying vertical load, one motor inside the wheel and one motor that pulls it. Tt is possible to impose a fixed slip ratio regulating the velocity induced by the two motors. Knowing that the vertical load and the slip ratio are the only two variables needed by

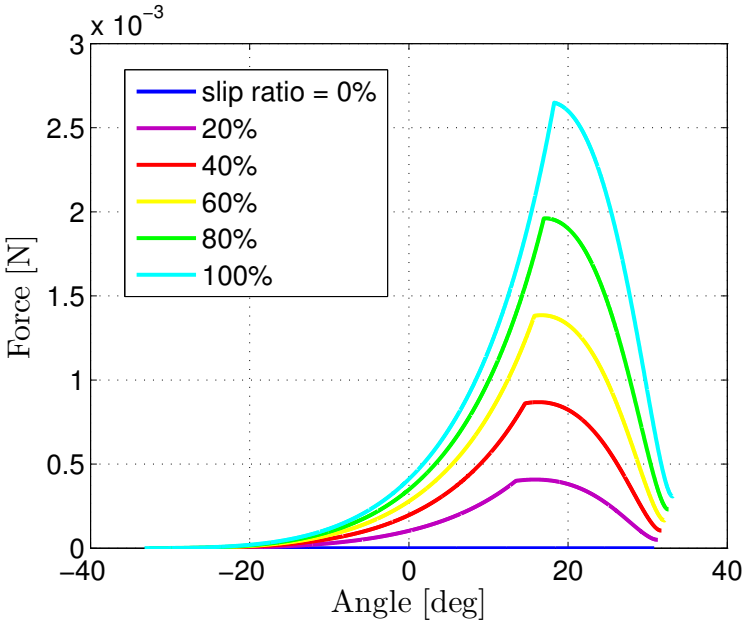

Figure 17: Force generated by one grouser in one rotation

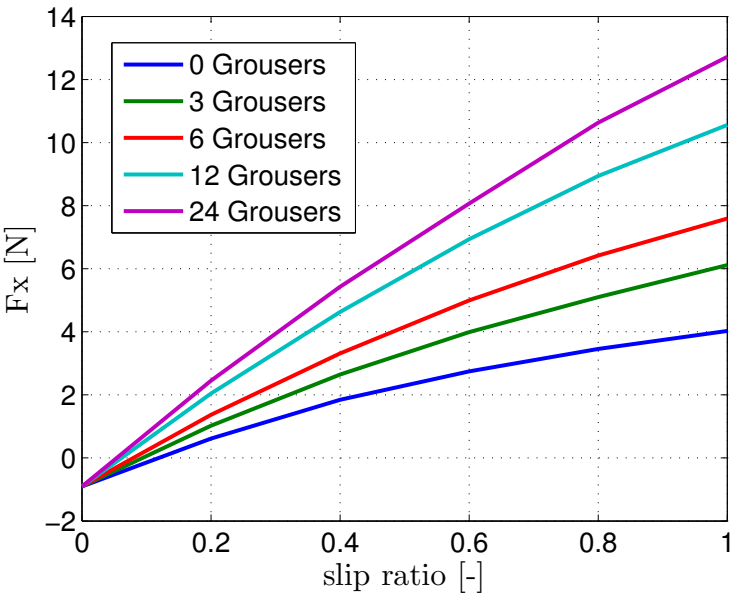

Figure 18: Drawbar pull for increasing number of grousers

the model, it is possible to verify every condition.

The test is performed inside a sandbox, which is 1.6 m in length, 0.3 m in width, and 0.2 m deep, filled with Toyura sand. Toyura sand has well known and controllable characteristics. The grain is almost homogeneous and the soil cohesion is almost zero. A wheel similar to the one mounted on the Moonraker is used for testing, since a replica is not provided. The wheel radius r is 125 mm, and the wheel width b is 100 mm. 12 grousers are fixed on the wheel surface at intervals

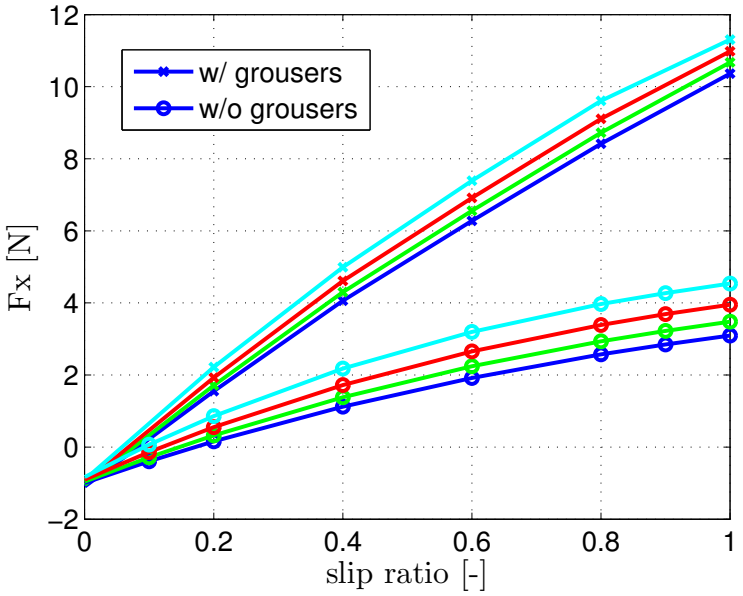

Figure 19: Drawbar pull comparison

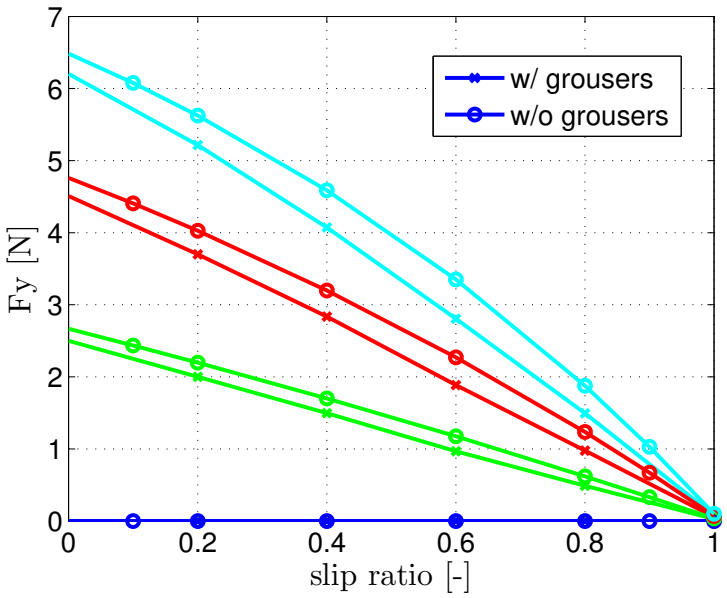

Figure 20: Lateral force comparison

of 30°, which are 25 mm in length, 5 mm in thickness, and 100 mm in width. The wheel-driving motor, embedded in the wheel, grants an arbitrary value of angular velocity.
A vertical structure holds the wheel in position. On it are mounted a steering mechanism, that forces the wheel to keep a determined slope angle β and a six-axis force/torque sensor located between the steering part and the wheel. The wheel-pully system ensures the longitudinal movement and the desired slip ratio.

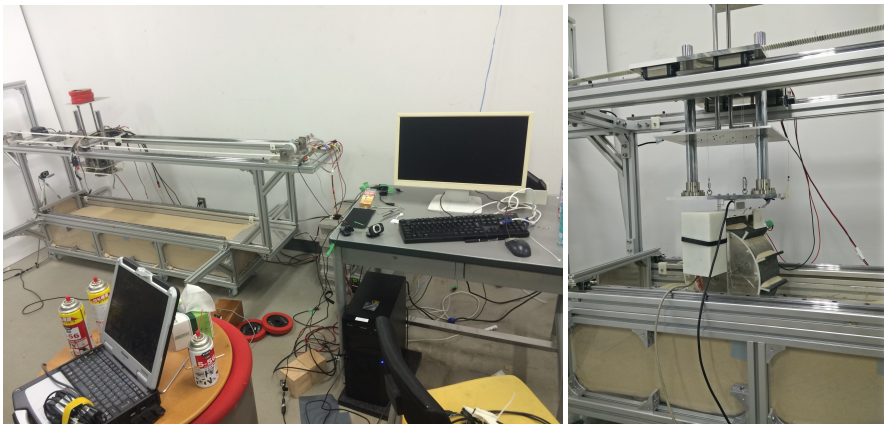

Figure 21: One-Wheel test setup

Several tests are performed in this environment: an average value for the drawbar pull and lateral forces are researched for slip ratio's value varying from 0 to 0.8, at interval of 0.2. This analysis is performed for β equal to 0° and 30° and different traveling velocities.
Figure 22 shows the raw data gathered from the F/T sensor for the drawbar pull.
The periodic effect that is evident in the picture, is due to the grou-

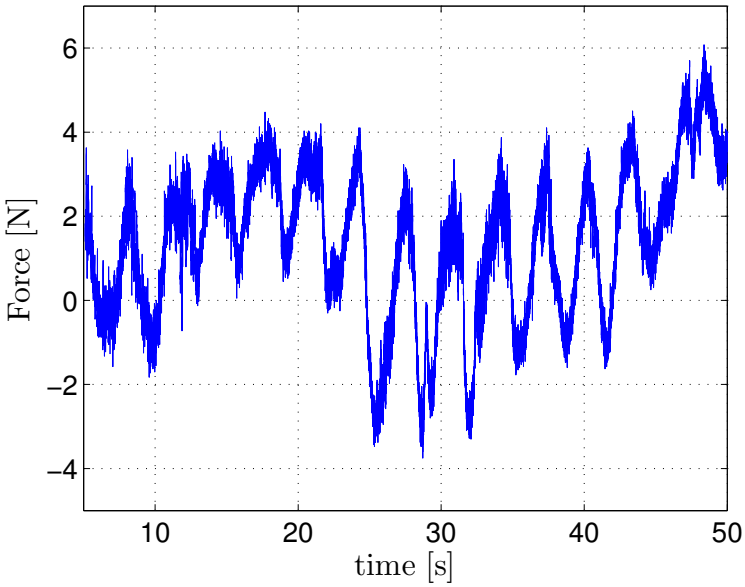

Figure 22: Drawbar pull measurement

sers acting on the soil at regular time interval.

2.15.1 *Velocity dependancy*

As already mentioned, the velocity of the rover is not a parameter of the wheel-soil model. Figure 23 and (24) show the experimental results. In the first it is shown the raw data obtained from the F/T sensor. Performing a time average and evaluating the standard deviation, it is possible to prove that there is not a proportionality with the velocity of the rover. This test also shows the increasing disturbance introduced for high velocity tests. Further tests are performed and the results shown in the following chapters.

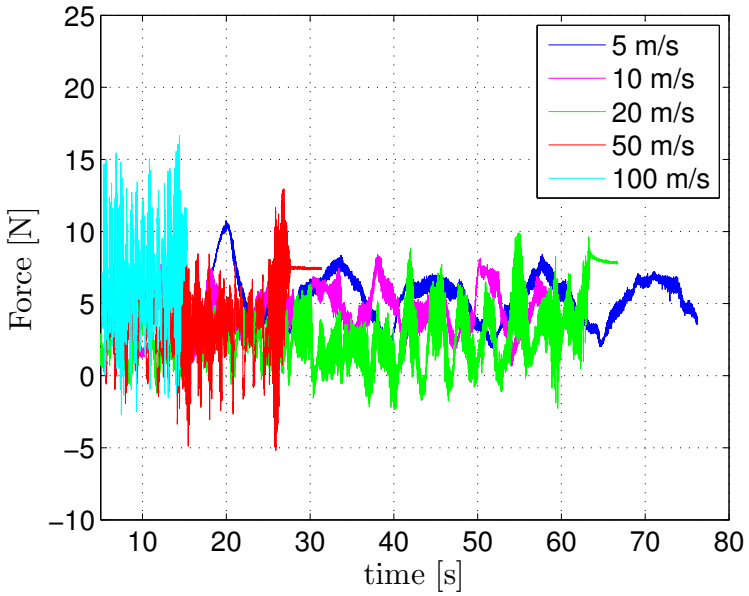

Figure 23: Drawbar pull rough data from F/T sensor for different velocities

2.15.2 *Results*

Figure 25 shows the comparison of the two models (without and with the grousers explicitly considered) with the results from the tests. The model that consider the grousers better estimates the shape of the force, underestimating it for high slip ratios.

The underestimation is more evident in the lateral force F_y, as shown in Figure 26. If the shape is well estimated, a systematic one Newton appears as offset from the test results.

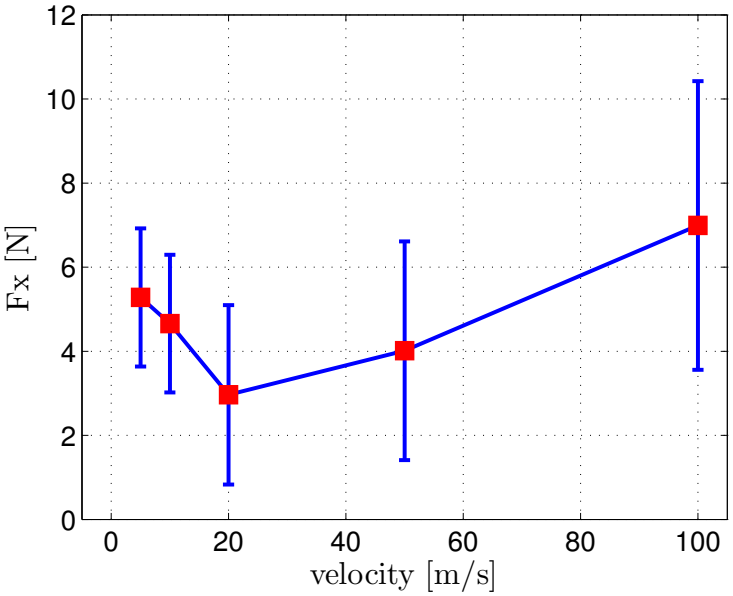

Figure 24: Drawbar pull analysed data at different velocities

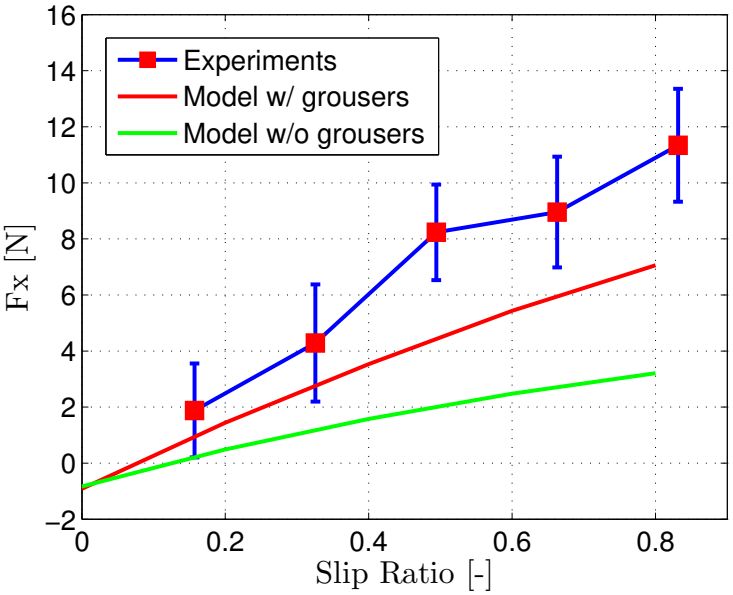

Figure 25: Models comparison with the test results

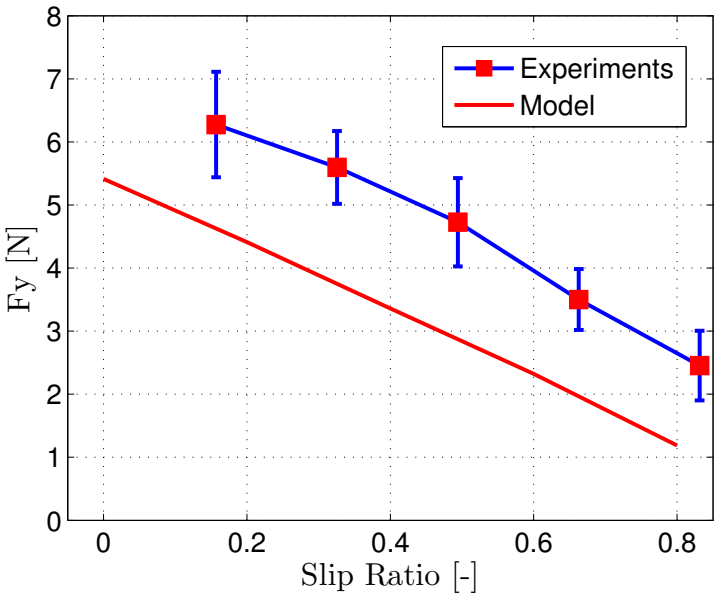

Figure 26: Lateral force comparison with the tests

3

DYNAMIC MODEL & NUMERICAL SIMULATION

In this chapter is firstly described how the Moonraker is modeled, and successively it is shown how this model is used, along with the wheel-soil model, to simulate the dynamic behaviour of the rover.

3.1 DYNAMIC MODEL

Moonraker has a pretty simple structure, without any flexible part, nor damping mechanism. It also does not have a steering mechanism. The only moving part is the arm on which the wheels are jointed. However, in this thesis, that degree of freedom is not considered, being its purpose is to ensure more mobility on rough terrain. As already said, one of the hypothesis for the framework is to have an homogeneous terrain.
According to what previously said, it is decided to model the rover as five concentrated masses, rigidly connected. Four masses describe the four wheels and a central mass is for the rest of the body. The forces resulting from the wheel-soil analysis act in the center of the wheel. Since the typical velocities for a rover are in the magnitude of few centimeters per second, the aerodynamic effects are neglected. The effect of the acceleration around the y_b axis is also considered negligible.
Being on flat surfaces (that can be with or without a slope) and having only small velocities and acceleration, the considered variables for the system are:

- x_i direction movement
- y_i direction momevent
- γ rotation around z_h axis
- θ_1 rotation of the front left wheel
- θ_2 rotation of the rear left wheel
- θ_3 rotation of the rear right wheel
- θ_4 rotation of the front right wheel

The subscript "*i*" is used to identify the different parts of the rover. It has values from 0 to 4, being 0 referred to the main body and from 1 to 4 to the wheels, numbered according to what described in the previously.

To obtain a precise physical description, with accurate values of masses and inertias, the CAD model, shown in Figure 27 and 28, is realized. Table 2 summarizes the used values. The four wheels are considered to be identical and the rover perfectly symmetrical along the longitudinal axis. The inertias reported are considered to be along the principal axis of inertia, that are aligned with the body reference frame.

Exploiting the hypothesis of rigidness, in Table 3 are listed the dis-

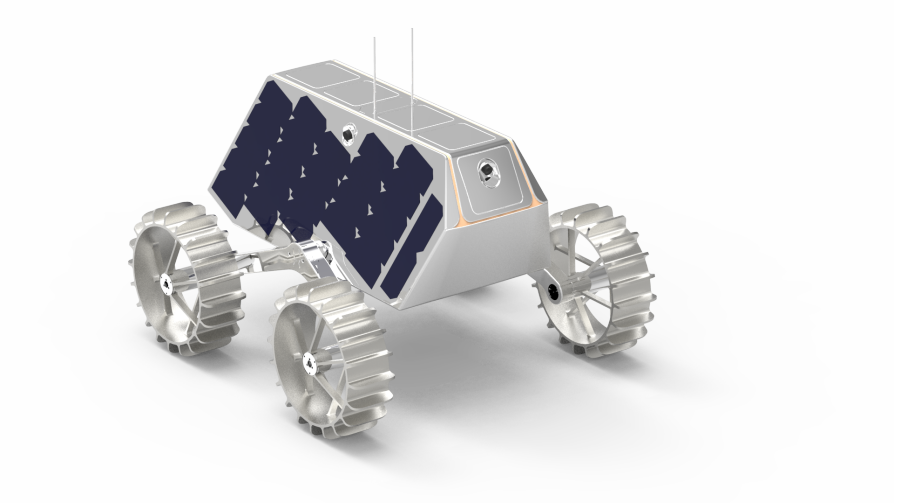

Figure 27: Moonraker EM: isometric view

	Mass [kg]	Ix [kg m^2]	Iy [kg m^2]	Iz [kg m^2]
Main Body	5.24	0.138	0.142	0.230
Wheel	0.422	0.00100	0.00154	0.00100

Table 2: Physical rover properties

tances of the center of mass of the five elements with respect to the origin of the body reference frame. The wheels are numbered from

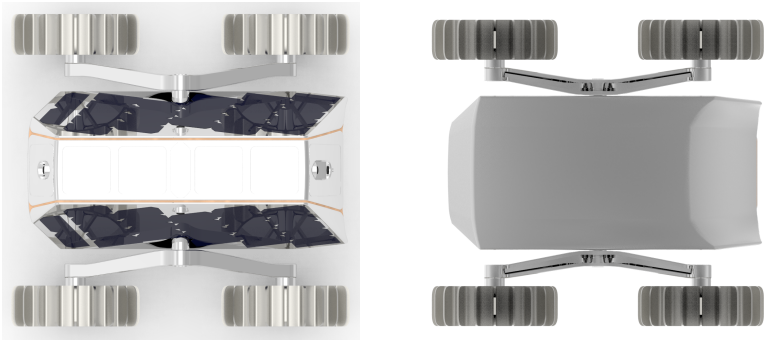

Figure 28: Moonraker EM upper and bottom view

the front-left in counterclockwise order (front-left is the wheel 1, rear-left is the wheel 2, rear-right is the wheel 3, front-right is the wheel 4).

The five bodies move along the x_h and y_h direction and rotate

	x [m]	y [m]	z [m]
Main Body	0	0	0
Wheel 1	0.19	0.24	-0.06
Wheel 2	-0.17	0.24	-0.06
Wheel 3	-0.17	-0.24	-0.06
Wheel 4	0.19	-0.24	-0.06

Table 3: Center of mass position

around z_h axis, for a total of fifteen variables, Adding the four wheels rotation θ, a total of nineteen variables are used to describe the dynamics.

An important effect of the rigidness hypothesis is the possibility to easily reduce the number of variables. The terms that refer to the main body are indicated by the subscript "*o*". The wheels variables are numbered accordingly to the wheel number (e.g. x_0, x_1, x_2). Not having a steering mechanism, all the rotations are equal, allowing the use of a single rotation angle γ. For what concerns the displacement variables, it is useful to link them to the central body displacement. Equations (45), (46) and (47) show how displacement, velocity and acceleration are defined.

$$\begin{cases} \underline{x}_i = \underline{x}_0 + \underline{\underline{A}}\,\underline{\tilde{x}}_i & \text{i=1,2,3,4} \quad (45) \\ \dot{\underline{x}}_i = \dot{\underline{x}}_0 + \underline{\underline{A}}(\underline{\omega} \times \underline{\tilde{x}}_i) & (46) \\ \ddot{\underline{x}}_i = \ddot{\underline{x}}_0 + \underline{\underline{A}}(\dot{\underline{\omega}} \times \underline{\tilde{x}}_i) + \underline{\underline{A}}\big(\underline{\omega} \times (\underline{\omega} \times \underline{\tilde{x}}_i)\big) & (47) \end{cases}$$

$\underline{x}_i$ is a 3x1 vector, containing the scalar component x_i, y_i, z_i.
$\underline{\underline{A}}$ is the rotation matrix, described by the angle γ.
$\underline{\omega}$ is the angular rotation vector $[0\ 0\ \dot{\gamma}]^T$.
$\underline{\tilde{x}}_i$ is the constant vector, having as elements the x distance, y distance and z distance described in the Table 3 (e.g. $\underline{\tilde{x}}_1 = [0.19\ 0.24\ -0.06]^T$).
To obtain the equations of motion, the Principle of Virtual Work (PVW) is computed and solved. The resulting solution in matrix form is reported in (48).

$$\underline{\underline{M}}\,\underline{\ddot{x}} = \underline{F} \quad (48)$$

$$\underline{x} = [x_0\ y_0\ \gamma\ \theta_1\ \theta_2\ \theta_3\ \theta_4]^T \quad (49)$$

$$\underline{\underline{M}} = \begin{bmatrix} m_{tot} & 0 & M_{x\gamma} & 0 & 0 & 0 & 0 \\ 0 & m_{tot} & M_{y\gamma} & 0 & 0 & 0 & 0 \\ M_{x\gamma} & M_{y\gamma} & M_{\gamma\gamma} & 0 & 0 & 0 & 0 \\ 0 & 0 & 0 & I_{w1} & 0 & 0 & 0 \\ 0 & 0 & 0 & 0 & I_{w2} & 0 & 0 \\ 0 & 0 & 0 & 0 & 0 & I_{w3} & 0 \\ 0 & 0 & 0 & 0 & 0 & 0 & I_{w4} \end{bmatrix}$$

$$\begin{aligned} M_{x\gamma} =& m_{wheel}((-\cos(\gamma)y_1 - \sin(\gamma)x_1) + (-\cos(\gamma)y_2 - \sin(\gamma)x_2) + \\ & (-\cos(\gamma)y_3 - \sin(\gamma)x_3) + (-\cos(\gamma)y_4 - \sin(\gamma)x_4)) \end{aligned} \tag{50}$$

$$\begin{aligned} M_{y\gamma} =& m_{wheel}((-\sin(\gamma)y_1 + \cos(\gamma)x_1) + (-\sin(\gamma)y_2 + \cos(\gamma)x_2) + \\ & (-\sin(\gamma)y_3 + \cos(\gamma)x_3) + (-\sin(\gamma)y_4 + \cos(\gamma)x_4)) \end{aligned} \tag{51}$$

$$M_{\gamma\gamma} = I_{0z} + 4\, I_{wz} + (m_{wheel}((x_1^2 + y_1^2) + (x_2^2 + y_2^2) + (x_3^2 + y_3)^2) + (x_4^2 + y_4^2))) \tag{52}$$

$$\underline{F} = \begin{bmatrix} F_x \\ F_y \\ F_\gamma \\ \tau_1 - T_{w_1} \\ \tau_2 - T_{w_2} \\ \tau_3 - T_{w_3} \\ \tau_4 - T_{w_4} \end{bmatrix}$$

$$\begin{aligned} F_x =& F_{x1} + F_{x2} + F_{x3} + F_{x4} + m_{wheel}(\cos(\gamma)x_1 - \sin(\gamma)y_1 \\ & + \cos(\gamma)x_2 - \sin(\gamma)y_2 + \cos(\gamma)x_3 - \sin(\gamma)y_3 \\ & + \cos(\gamma)x_4 - \sin(\gamma)y_4)\dot{\gamma}^2 \end{aligned} \tag{53}$$

$$\begin{aligned} F_y =& F_{y1} + F_{y2} + F_{y3} + F_{y4} + m_{wheel}(\cos(\gamma)y_1 + \sin(\gamma)x_1 \\ & + \cos(\gamma)y_2 + \sin(\gamma)x_2 + \cos(\gamma)y_3 + \sin(\gamma)x_3 \\ & + \cos(\gamma)y_4 + \sin(\gamma)x_4)\dot{\gamma}^2 - \sin(\alpha)\, m_{tot}\, g \end{aligned} \tag{54}$$

$$\begin{aligned} F_\gamma =& ((-\cos(\gamma)y_1 + \sin(\gamma)x_1)F_{x1} + (\sin(\gamma)y_1 + \cos(\gamma)x_1)F_{y1}) \\ & + ((-\cos(\gamma)y_2 + \sin(\gamma)x_2)F_{x2} + (\sin(\gamma)y_2 + \cos(\gamma)x_2)F_{y2}) \\ & + ((-\cos(\gamma)y_3 + \sin(\gamma)x_3)F_{x3} + (\sin(\gamma)y_3 + \cos(\gamma)x_3)F_{y3}) \\ & + ((-\cos(\gamma)y_4 + \sin(\gamma)x_4)F_{x4} + (\sin(\gamma)y_4 + \cos(\gamma)x_4)F_{y4}) \\ & + T_{z1} + T_{z2} + T_{z3} + T_{z4} \end{aligned} \tag{55}$$

The considered system has seven variables, but the wheel's rotations are fully decoupled from the rest of the system.
τ_i are the torques given by each wheel motor. It might look bizarre, but it has an explanation in the structure of this model. The link between the wheel rotation and the main body is implicit in the forces acting on the main body itself. The wheel rotation determine a certain slip ratio. Due to that, forces and torques are generated on the wheel and transmitted to the rest of the structure. As expected, it is not present an elastic element, nor a viscous one. A velocity non-linear term, and a gravitational term are recovered.

3.2 NUMERICAL SIMULATION

Through the usage of MATLAB® and SIMULINK® is created an environment that simulates the motion of the rover. It is composed by three major blocks:

- Motor controller: it controls the torque given by the wheels motors to grant a certain wheels velocity. Two approaches are studied in this thesis and later presented in this chapter
- Dynamics: it has as input the forces and torques generated by the wheel-soil interaction and eventually the torque granted by the wheels motors. The output is the dynamic variables of the system
- Wheel-soil: it traduces the wheels velocity, rover velocity and physical properties into the forces acting in the system.

3.2.1 *Simulation objectives*

Being this work part of a bigger project, one of the imposed requirement is to create a tool that predicts the behaviour of the rover on loose soil, keeping fixed input conditions. The reason for that can be found in the operational modes of the rover and in the used software. The rover is programmed to perform short distances following a straight line, and keeping a specific velocity, or to perform a spot turn of a certain angle. MATLAB® has the limit of being computational demanding, making it impossible to be used on the on-board computer. Moreover, the only input of the on-board software is the wheel velocity. The purpose of this tool is to find the proper angular velocity for each wheel, that can be used in a real case scenario.
For this reasons there is not a true control design, but more properly a research for the optimal initial attitude and input for the motor controller.

3.2.2 *Torque input & Velocity input*

Torque input

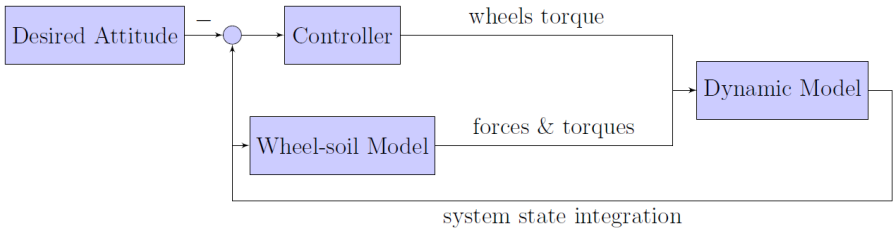

Figure 29: Torque input strategy scheme

Two input approaches are discussed. The so called *torque input* is firstly implemented. It is based on a PD control (described in (56)) that observes the state and compares it with a desired one. In this thesis, the desired state is described by a specific velocity in the longitudinal direction, that is exactly what would be expected on rigid terrain.

$$\tau_i = k_p \, \Delta v + k_d \, \Delta a \tag{56}$$

The difference between the actual and the desired velocity is defined as Δv and the difference between the actual and the desired acceleration is defined as Δa.
The parameters k_p and k_d are experimentally tuned.
This produces a value of the four torques varying in time that ensures the desired state. For the reasons explained above, this is not what can be used in a real environment. The wheel velocity must be averaged over the simulation time, and that becomes the usable input for the on-board software.

Velocity input

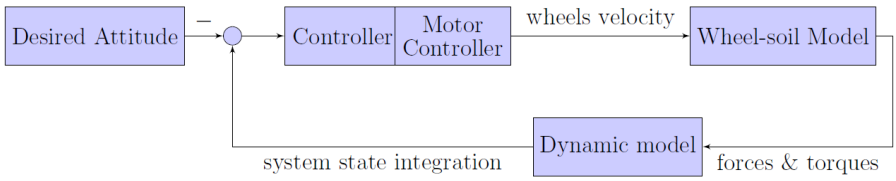

Figure 30: Velocity control strategy scheme

A different approach is proposed, that is closer to the actual needs of for the real tests. Having in mind that the final goal is to predict the trajectory, and a motor controller is already present in the rover, it is easier to impose the wheels velocity to the simulation. For practical applications, it is also the only possible solution. In our system, it is not possible to monitor and control the input current in the motor by now. A steady velocity input is therefore the more reasonable choice

also for the simulation. Knowing that the velocity of the wheel is not the velocity at which the rover will travel, it is proposed a way to determine the desired velocity to impose to the rover.
Starting from the definition of the slip ratio and fixing the desired velocity v_{des} and a reference slip ratio s_{ref}, the only variable results the wheel velocity. The reference slip ratio s_{ref} is assumed to be 0.2. It is experimentally demonstrated that this is a common value at which the rover slip ratio converges in steady state. The used equation is the (57).

$$\omega_i = \frac{v_{des}}{(1-(s_{ref}-s))*\cos(\gamma)*r} \tag{57}$$

Particular attention must be put to the fact that using this approach, the dynamics of the wheels is no more handled by the tool, but it is granted by the on-board computer. The elements of (48) are here redefined.

$$x = [x_0\ y_0\ \gamma]^T \tag{58}$$

$$\underline{\underline{M}} = \begin{bmatrix} m_{tot} & 0 & M_{x\gamma} \\ 0 & m_{tot} & M_{y\gamma} \\ M_{x\gamma} & M_{y\gamma} & M_{\gamma\gamma} \end{bmatrix}$$

$$\underline{F} = \begin{bmatrix} F_x \\ F_y \\ F_\gamma \end{bmatrix}$$

3.2.3 *Simulation procedure*

In this section it is explained how to perform a simulation with this tool. As before, the values for the soil parameters and dimensions of the wheels used in the simulations are left to a dedicated chapter that follows.

1. The fixed parameters are set. The slope of the terrain α, geometry of the rover x_i, masses m_i and inertias I_{ix}, I_{iy}, I_{iz}, desired velocity: v_{des}
2. Set the soil parameters (c,n,k_c,k_ϕ,ϕ,ρ,κ), the wheel parameters (r,b) and the normal load W.
3. Set the initial state to be used in the first iteration.
4. The wheel-soil model evaluates the slip ratio s and gives as output the forces and torques acting on the system.
5. The dynamic model recives the forces and evaluated the state in the following time step. The obtained equations of motion is solved using Simulink®.

6. Enter the obtained state at point 4. and iterate.

The flowchart (31) summarize the solving process.

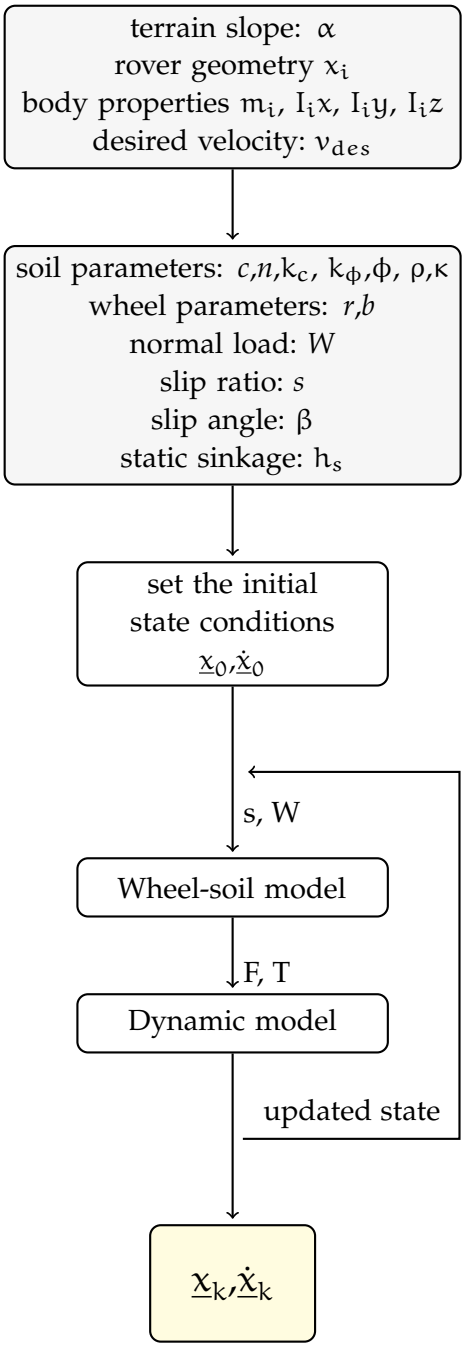

Figure 31: Numerical simulation flowchart

3.2.4 *Numerical simulation optimization*

The described motion can be highly dynamic, requiring for really small integration steps. Having to evaluate the forces for each wheel,

for every time step, this computation can be highly time consuming. With the described standard procedure, it can take up to 24 hours for a single second of simulation on a personal computer.
Being the reaction forces evaluated in a deterministic way, having few input variable, to dramatically increase the computational speed, it is generated a set of 3-dimensional matrices, where all the possible combination of input are considered, and the resulting forces are saved. Doing this, the code simply selects the right variables for the time step and retrieves the forces from the presaved matrix. The variables used for each matrix are the slip ratio s and the slip angle β. The slope α is kept as parameter for each simulation. It is not selected as variable, since the value of α is constant during each simulation, and few values are used in this thesis (the considered slopes are 0°, 5°, 10°, 15°, and 20°). A region of interest for those 2 variables is defined (from -1 to 1 for the slip ratio and $-90°$ to 90° for β). A certain level of accuracy must be selected, defining how many points within the range of interest are to be evaluated. The accuracy can be highly increased performing an n-dimensional interpolation within the points of the matrix. The used MATLAB® function is *interpn*.
Depending on the point density, the production of the matrices can take hours to compute. One second of simulation takes minutes to compute, once the desired force matrix is available. The suggested procedure is summed thereafter and the corresponding flowchart in 32.
Firstly the force matrix is created:

1. Set the soil parameters (c,n,k_c,k_ϕ,ϕ,ρ,κ,α), the wheel parameters (r,b) and the normal load W
2. A vector containing all the desired values of slip ratio s and the slip angle β is defined
3. Select a combination of values of slip ratio s and slip angle β
4. Determine the sinkage h with an iterative procedure, increasing the dynamic sinkage until the vertical load W is balanced by the vertical force F_z
5. Calculate the contact angles θ_f and θ_r
6. Evaluate the normal stress σ, the shear stress τ_x and τ_y
7. Calculate the resulting forces F_x, F_y, T_y,T_z
8. Save the results in the corresponding matrix location and return to 3.

The simulation is performed as:

1. The fixed parameters are set. The geometry of the rover x_i, masses m_i and inertias I_{ix}, I_{iy}, I_{iz}, desired velocity: v_{des}

2. The proper force matrix is loaded.
3. Set the initial state to be used in the first iteration.
4. Evaluate the slip ratio s and the slip angle β. Select the corresponding forces and torques from the force matrix.
5. The dynamic model receives the forces and evaluated the state in the following time step. The obtained equations of motion is solved using SIMULINK®.
6. Enter the obtained state at point 4. and iterate.

3.3 SIMULATIONS

The main interest of this thesis is to analyze the traverse motion of the rover. The simulations performed are aimed to better predict and eventually correct the motion in this kind of operations. The variables for the simulations are the slope of the terrain, the angle γ, that is defined as the angle between the x_h axis and x_b, initial state and desired velocity (as explained before it has little effect). Figure 33 and 34 show an example of the simulated motion in the case of γ equal to zero and 10° sloped terrain.

The resulting motion is linear, having a slip angle β determined by the slope of the terrain. This peculiarity is due to the force balance. The motion starts as horizontal, but along y_h acts a component of the gravity, making the rover accelerate in the same direction. The change of velocity determines an increasing value of β, that results in and increase of lateral force, until an equilibrium, that keeps the lateral velocity constant, is reached. Thanks to this, it is possible to simulate short distances to know the behaviour of longer distances. This equilibrium condition is verified also through the other outputs of the model. Figure 35 is shown as example for the initial transient and effectiveness of the wheel velocity determination. The initial slip ratio equal to one identifies the moment in which the rover is still, and the wheel start rotating.

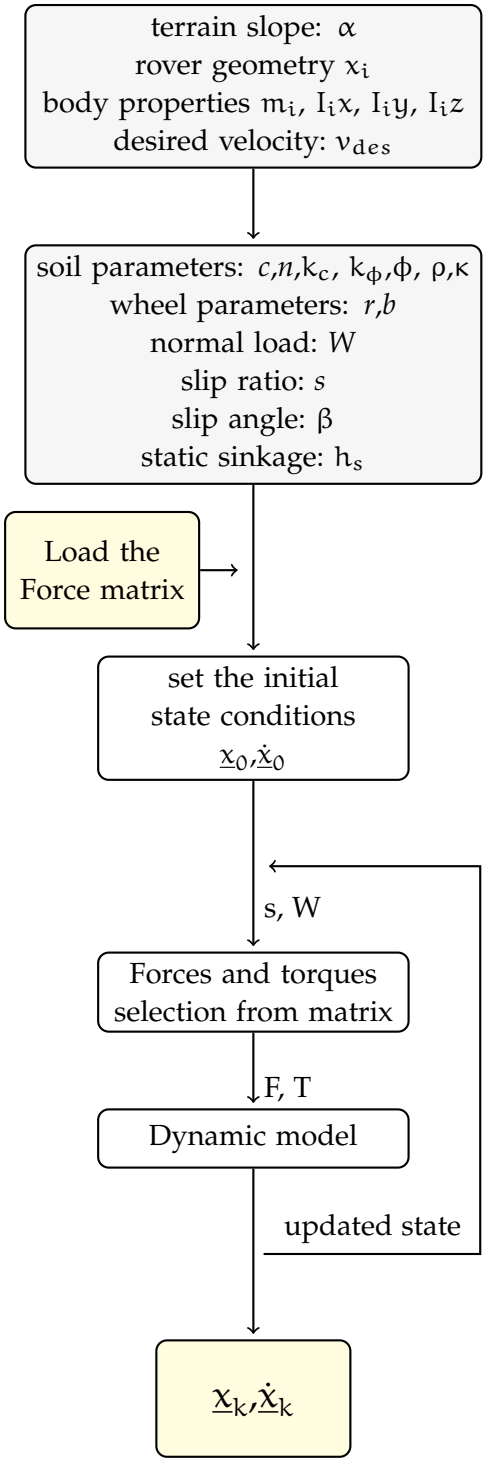

Figure 32: Optimized numerical simulation flowchart

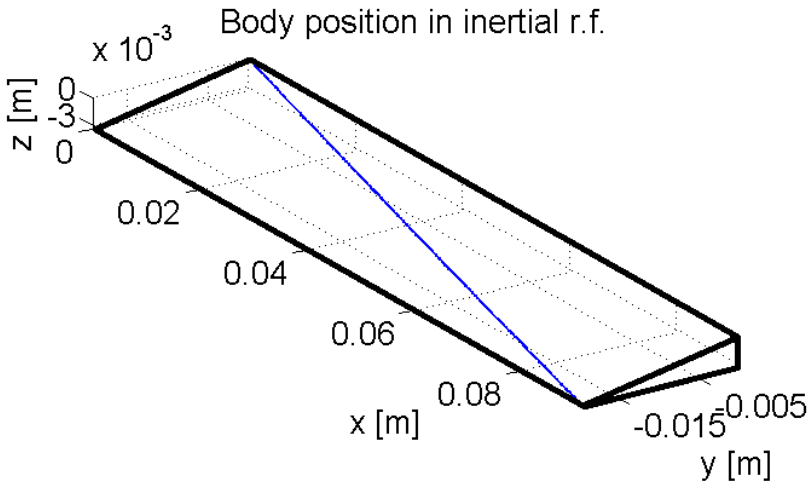

Figure 33: Example of motion on sloped terrain

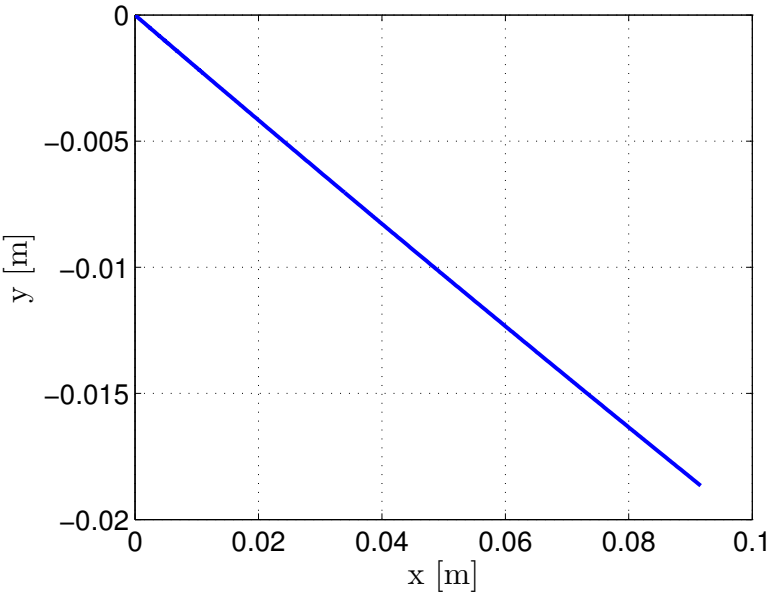

Figure 34: Example of motion on sloped terrain

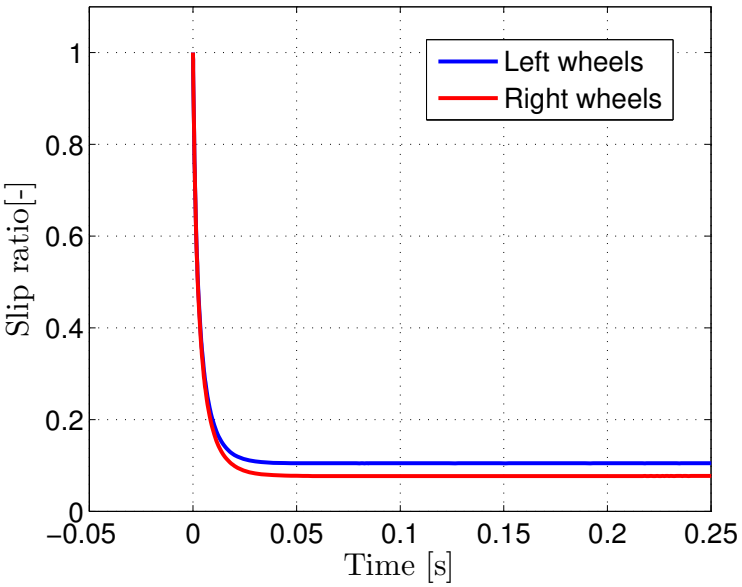

Figure 35: Slip ratio transient

4 RESULTS

In this chapter, the built model is used to verify the goals of this thesis. The simulated dynamics is compared with test performed with the Moonraker in a controlled environment and in a natural environment. Successively it is proposed a method to compensate the lateral slip for operations on loose soil.

4.1 TESTING

In this thesis work, three tests are performed:

- **One-wheel** testing, already discussed in Section (2.15), is performed to compare the results of the Wheel-soil model with the values arising from testing. The setup of this test is a wheel, with varying vertical load, one motor inside the wheel and one motor that pulls the wheel. Regulating the velocity induced by the two motors, it is possible to impose a fixed slip ratio. Knowing that the vertical load and the slip ratio are the only two variables needed by the model, it is possible to verify every condition.
- **Sandbox** testing is performed to verify the performance of the tool, predicting the behaviour of the rover moving on loose soil. Tests are performed for different slopes. The setup consist in a rectangular box filled with Toyura sand and the Moonraker PFM2 traversing it.
- A **field test** is also shown to demonstrate the sensibility of the model to the terrain characteristics. Moonraker PFM2 is moved on a beach and the mobility on an inhomogeneous terrain is compared with the results on controlled environment terrain.

4.1.1 *Sandbox*

Figure 36 shows the environment of this test.
The sandbox is a 2.0 m in length, 1.0 m in width, 0.08 m deep tiltable vessel, filled with Toyura sand.
The rover used in this tests is the Moonraker PFM2: it weights about 7 kilograms, the wheels are 9 centimeters in radius and 8 centimeters

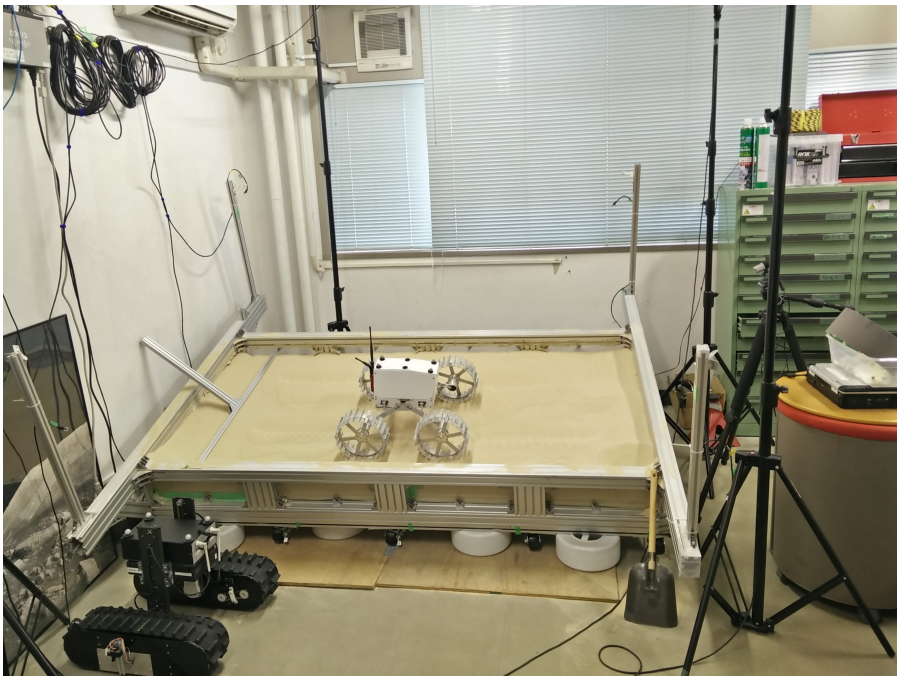

Figure 36: Sandbox test setup

in width. 15 grousers are fixed to the wheel, being 2 centimeters long and 8 centimeters in width.
The test data are acquired through the use of four motion capture cameras (Stereo Labeling Camera developed by CyVerse Corp.). Those cameras can track the position of specific reflectors mounted on the rover. Computing the derivative of the position in time, also the velocity can be retrieved.
In this environment, the traversing capabilities are tested. According to how the horizon reference frame is defined, different initial rotation angle γ are tested, on flat surface, 5° slope, 10° slope and 20° slope, at different velocities. The results are then compared to simulated one, to verity the precision of the model. It is important to underline that minor differences and error can be due to setup errors: dealing with small angles, even few degree of error in the placement the rover in position, can lead to significant errors in the results.

4.1.2 *Model tuning*

In an ideal condition, where the proposed model perfectly describes the reality, it could be used to simulate the rover trajectory.
To verify the accuracy of the model, a test campaign is performed in the sandbox for 10° and 20° slope angles.
The first test is performed with the initial angle γ equal to zero. If the side slip is absent, this configuration should lead the rover to traver-

sing the slope. In Figure 37 and 38 are shown the comparison between the trajectory recorded by the optic trackers and the simulation.
The model highly overestimates the side slip. This difference is intro-

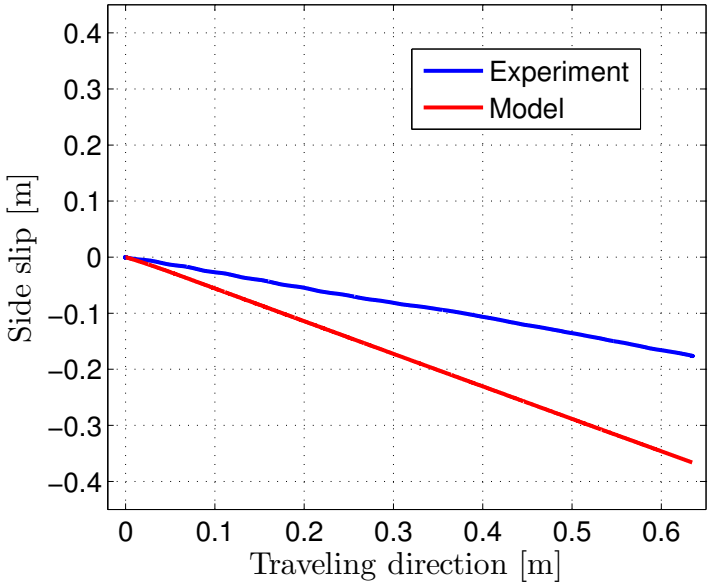

Figure 37: Comparison of the model for 20° slope

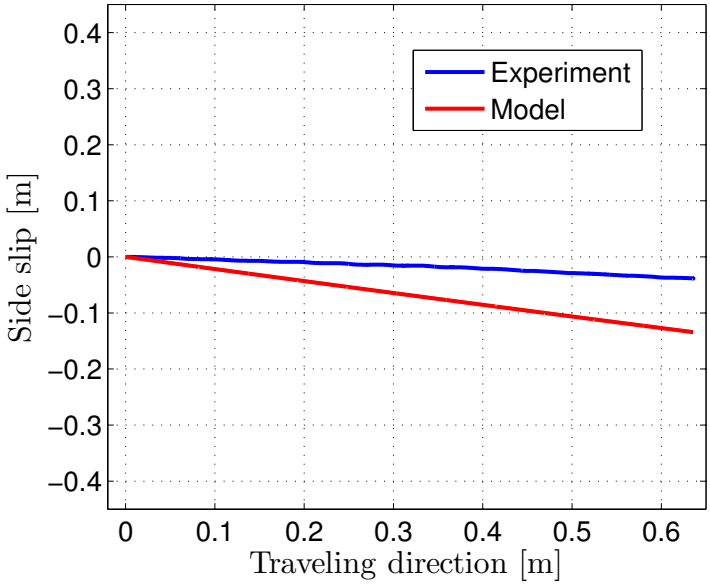

Figure 38: Comparison of the model for 10° slope

duced by errors in the Wheel-soil model and in the dynamics mode (as shown in Figure 26), the lateral force is underestimated)l.
An essential part in the creation of a model that has to be used in real test is the tuning. The optimal tuning of a multi-parameter model

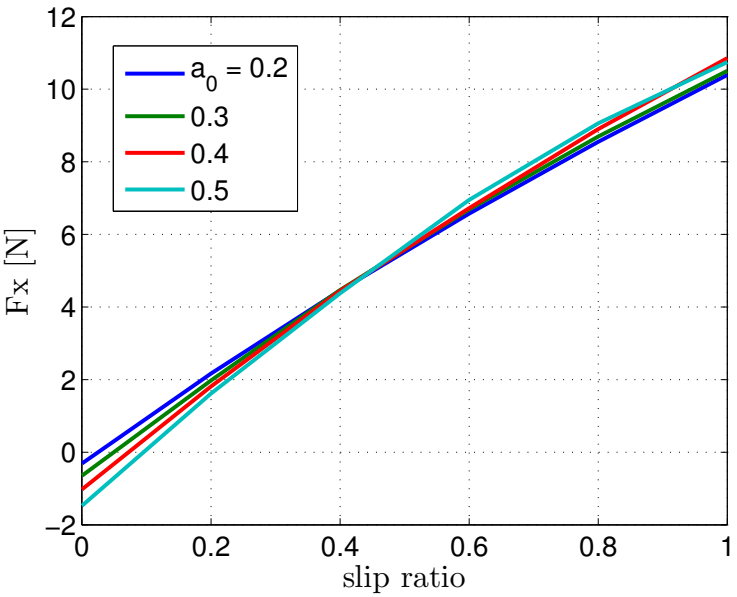

Figure 39: Model sensitivity to parameter a_0

would require a dedicated study, that is not of interest for this thesis. This model is based on many empirical variables, related to different aspects of the system. The mismatch in the results can be due to a erroneous evaluation of one or more of those parameters. Being the goal of this thesis to properly simulate the behaviour of a specific kind of vehicle, the model sensibility to the parameter is thereafter verified. The chosen values interval, to verify the sensitivity, is taken considering the commonly used values for the Toyura sand, found the in the literature. It is stressed that in this procedure, it is no more relevant to use the correct values of the single parameters, being more interested in the global results.

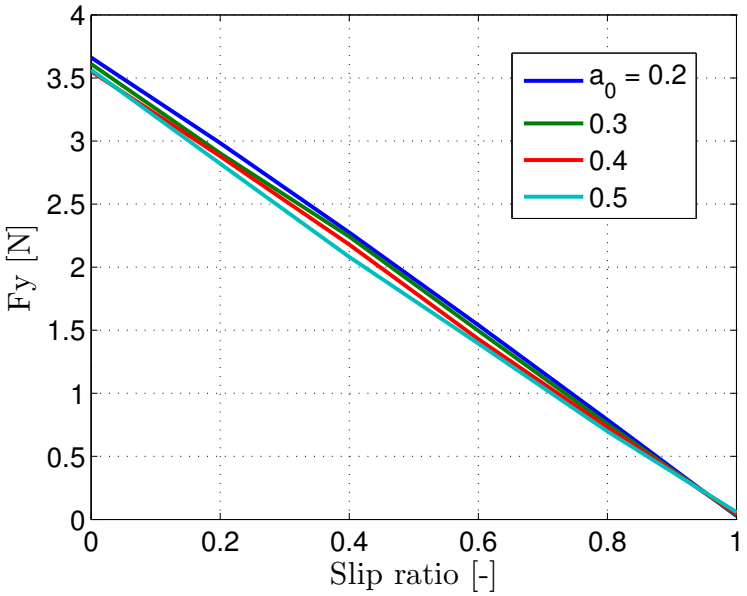

Figure 40: Model sensitivity to parameter a_0

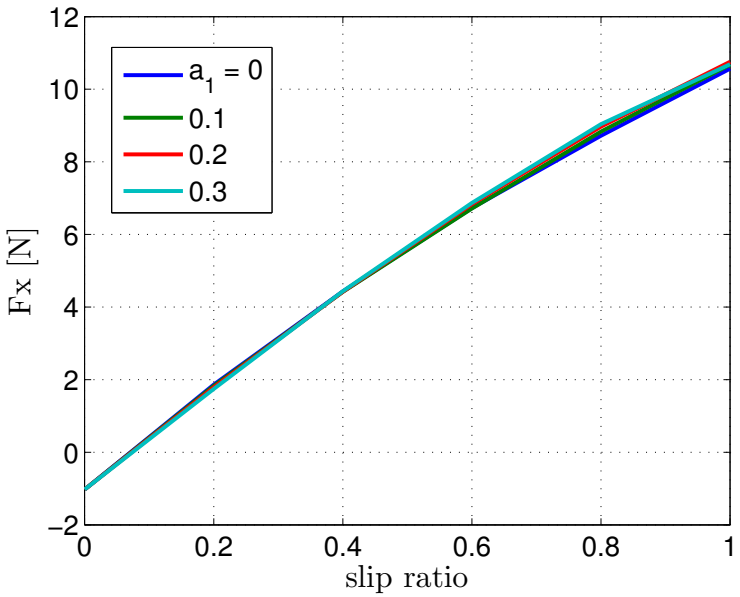

Figure 41: Model sensitivity to parameter a_0

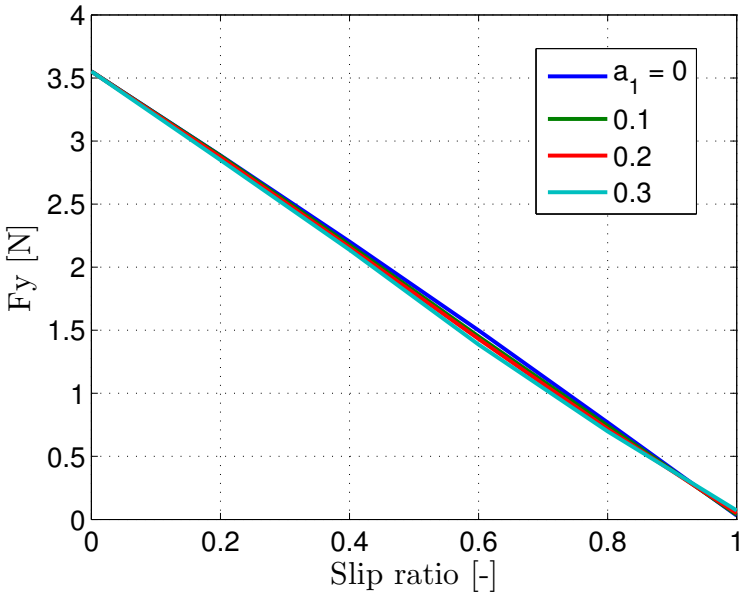

Figure 42: Model sensitivity to parameter a_1

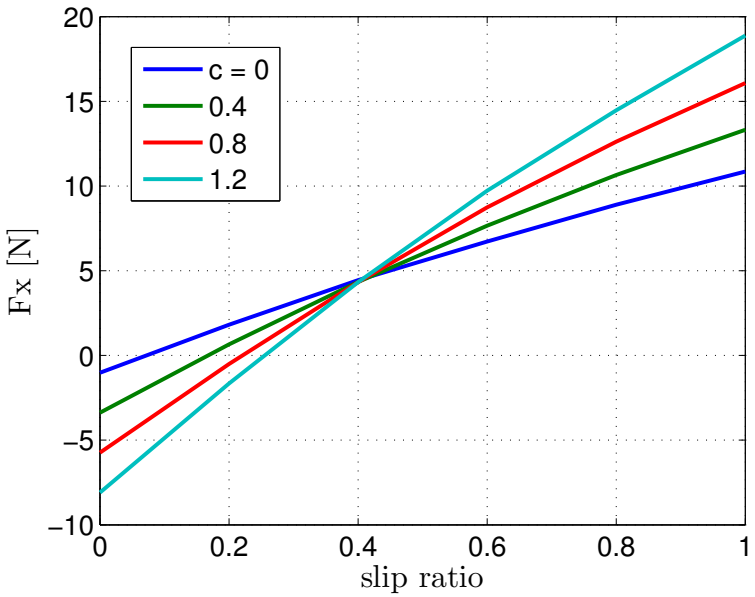

Figure 43: Model sensitivity to parameter a_0

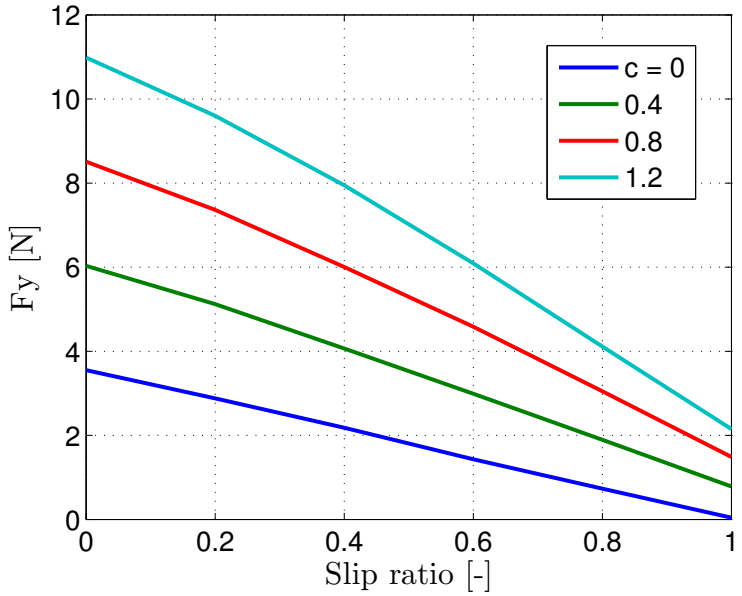

Figure 44: Model sensitivity to parameter c

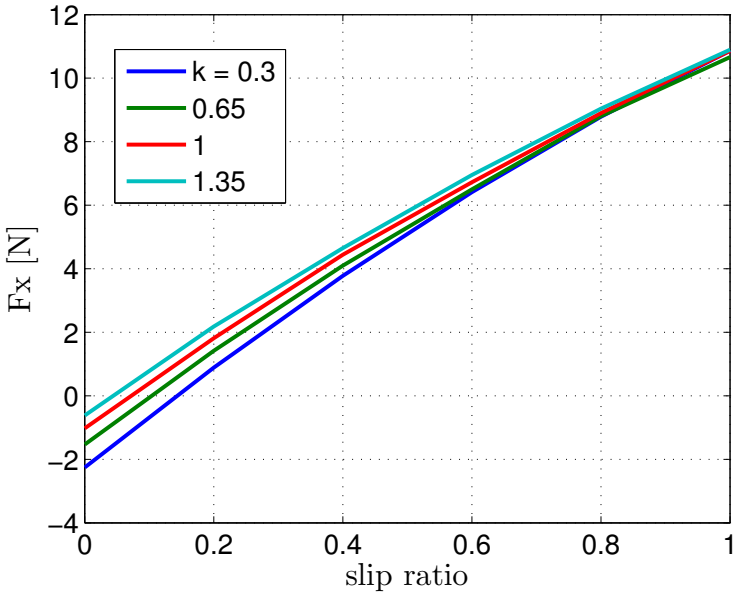

Figure 45: Model sensitivity to parameter a_0

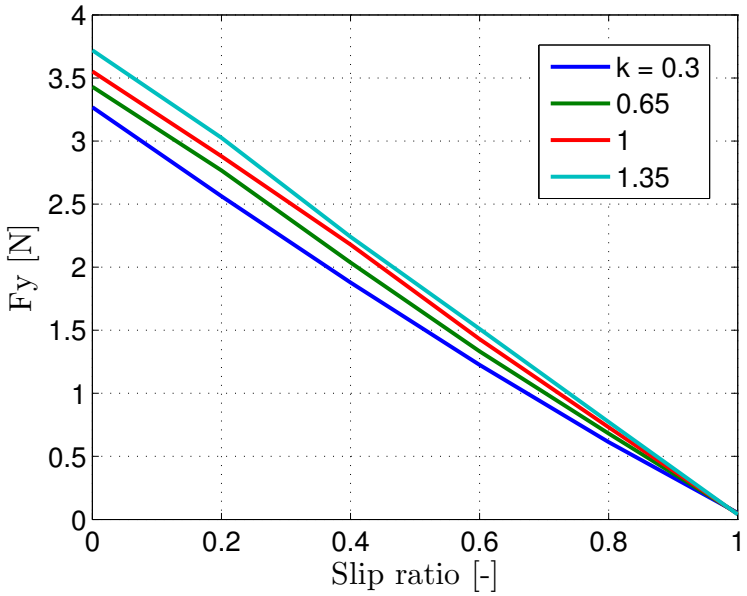

Figure 46: Model sensitivity to parameter κ

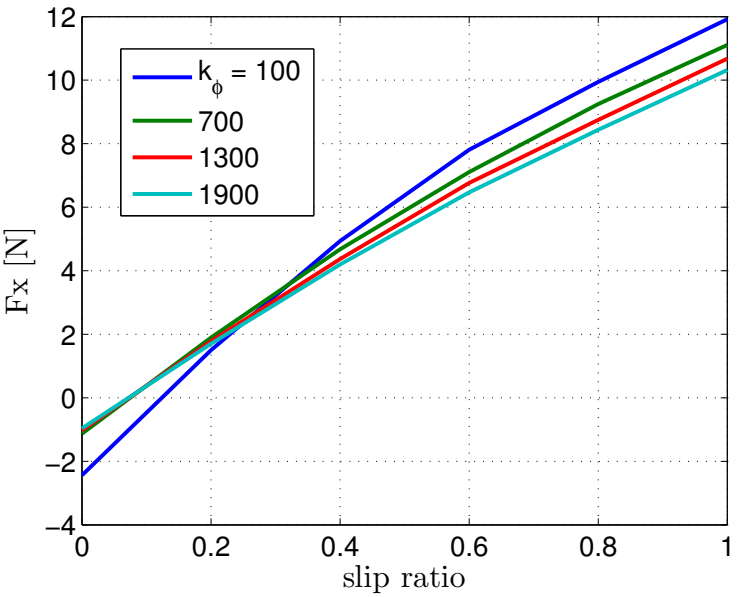

Figure 47: Model sensitivity to parameter a_0

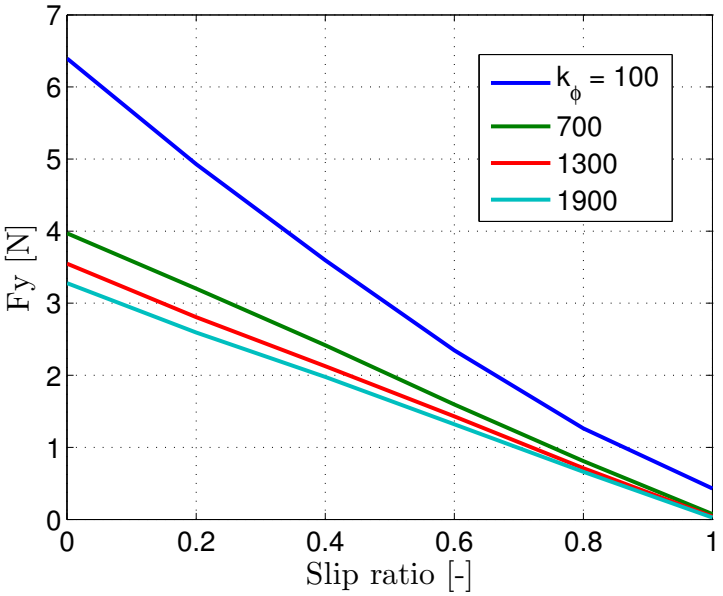

Figure 48: Model sensitivity to parameter k_ϕ

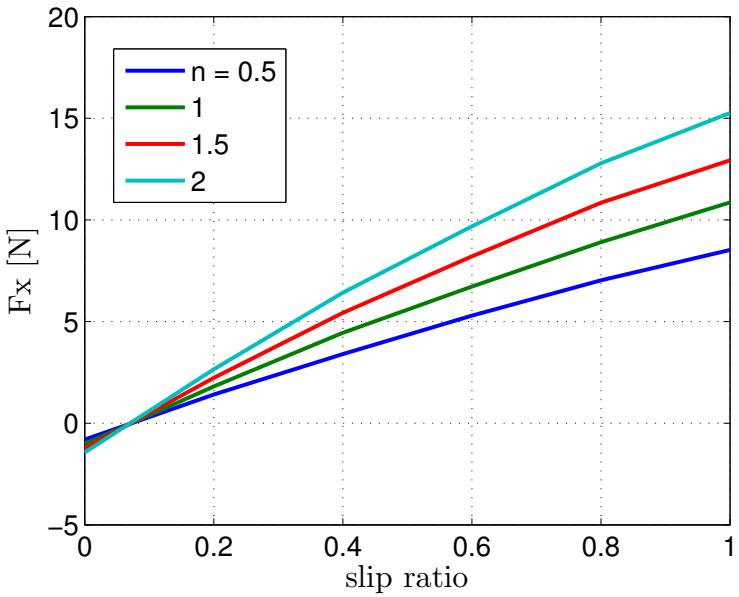

Figure 49: Model sensitivity to parameter a_0

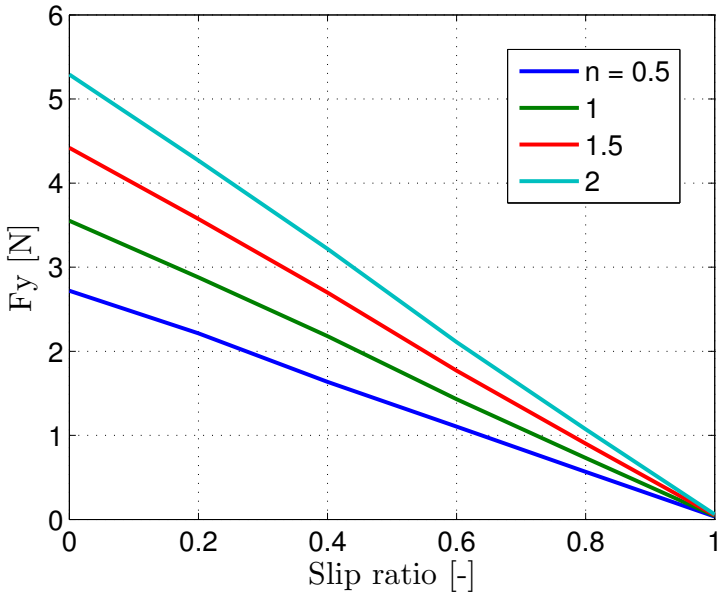

Figure 50: Model sensitivity to parameter n

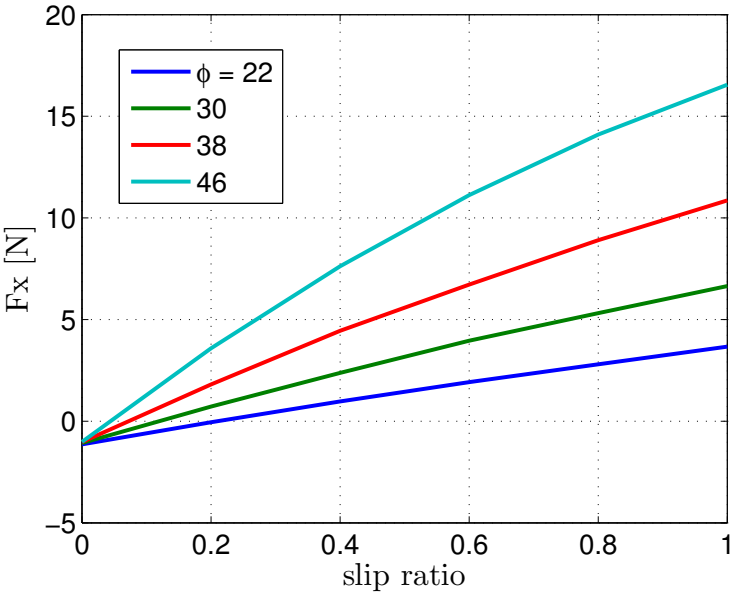

Figure 51: Model sensitivity to parameter a_0

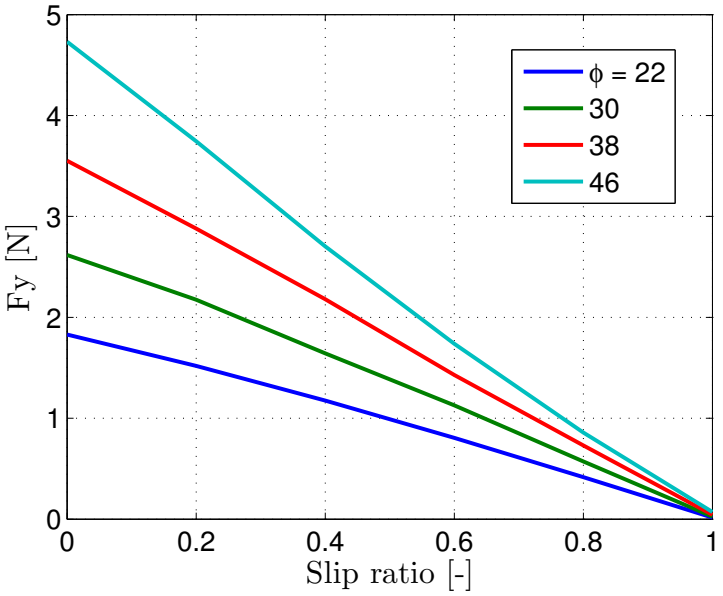

Figure 52: Model sensitivity to parameter ϕ

The value of the cohesion, c, is changed from 0 to 0.4 kPa. It is stressed that this doesn't have a physical meaning, but it is just used to properly fit the model with the reality. Figure 53 and 54 show that changing a single parameter is enough to better fit the results obtained from the F/T sensor.

The model is again verified in Figure 55 and 56. Being the model still

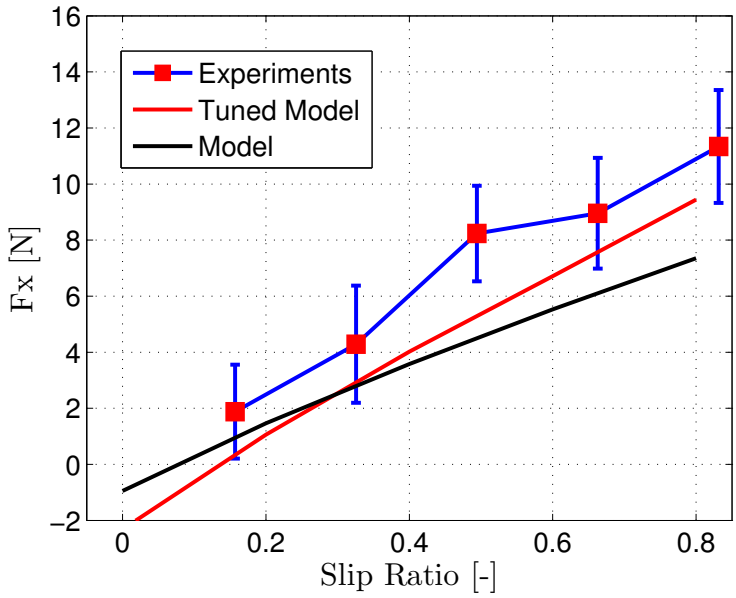

Figure 53: Tuning of the wheel-soil model

far from being acceptable, the error is now addressed to the dynamic

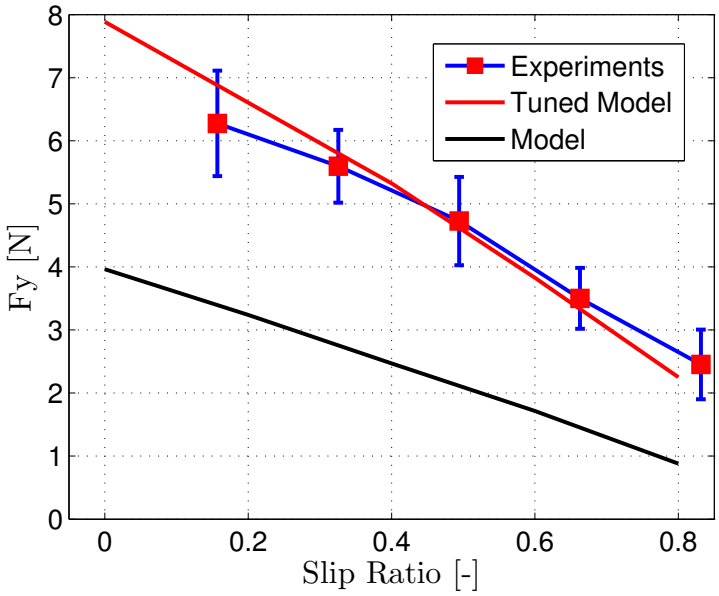

Figure 54: Tuning of the wheel-soil model

model. Using a similar strategy to what adopted for the wheel-soil model, the weight of the rover is chosen to be the appropriate parameter to be changed. It is therefore lowered of 20%. Figure 57 and 58 show the effect of this change.

The simulation error is evaluated as ratio between the difference in

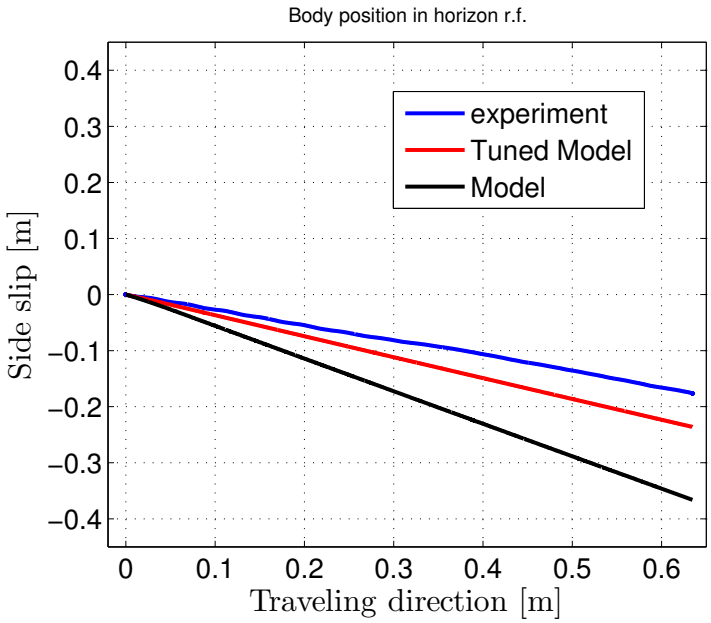

Figure 55: Effect of the force tuning on the dynamics

the side slip and the traveled distance. Table (4) sums the simulation error at each tuning step.

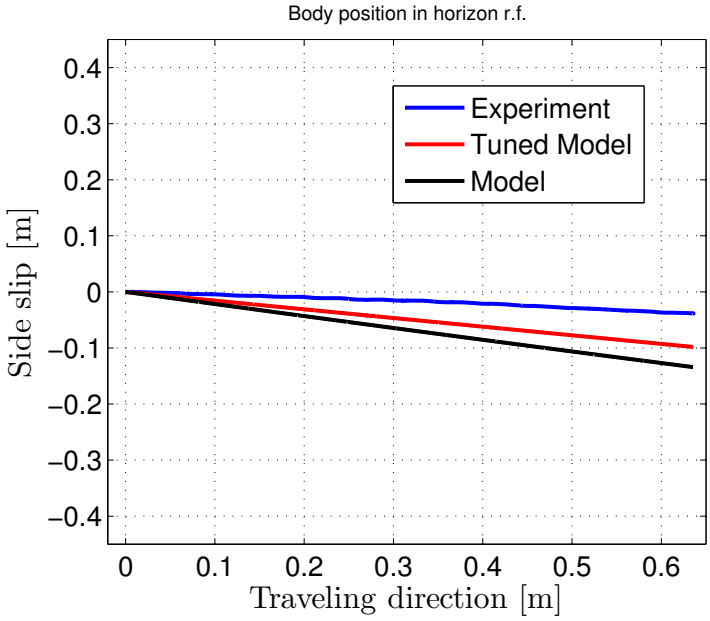

Figure 56: Effect of the force tuning on the dynamics

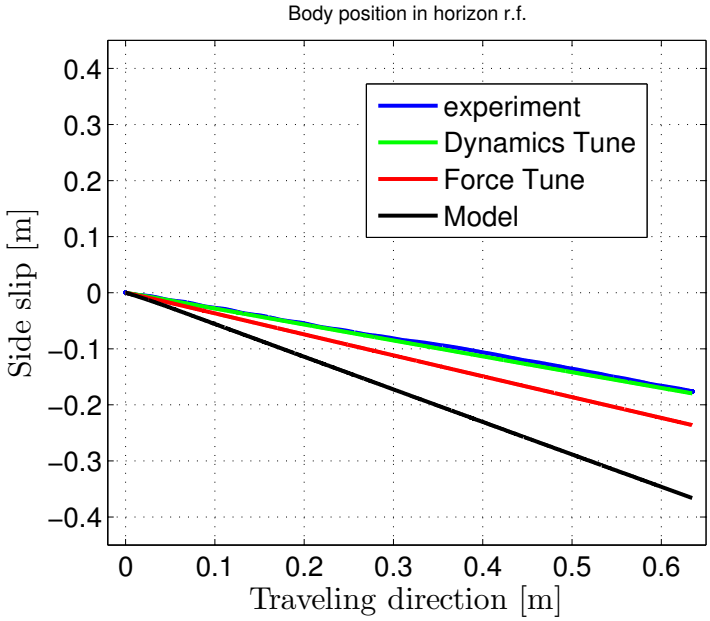

Figure 57: Tuning of the dynamic model

For this example of tuning, the focus is given on the 20° slope case, obtaining a final error of less than one percent. Using the same tuned model, the other case under study sees its error more than halved, being its final value around six percent.

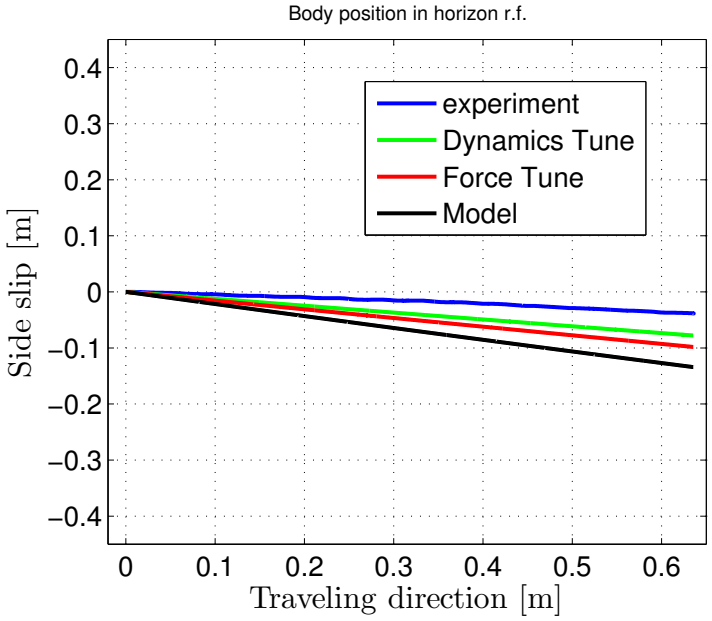

Figure 58: Tuning of the dynamic model

	10°slope	20°slope
Base model	14.76%	25.91%
Force tune	9.32%	8.82%
Dynamic tune	6.17%	0.49%

Table 4: Simulation errors

4.1.3 *Velocity correlation*

As previously demonstrated through the results of the one-wheel tests, also using the sandbox it is possible to demonstrate that the velocity does not affects the motion. In Figure 59 and 60 two tests are compared. The two run are performed imposing a velocity to the rover of respectively with around 3 cm/s and 10 cm/s. Especially in the second image it is evident the unrelevance of the velocity on the trajectory. More tests are being performed, to have a wider data sets to analyze.

4.2 FIELD TEST

The mobility of the Moonraker is tested at the Sendai beach on uncontrolled sand.

While the main achievements of the field test were correlated to the communication system, there was also the occasion to perform mobility tests. The equipment used for this test are the ground control

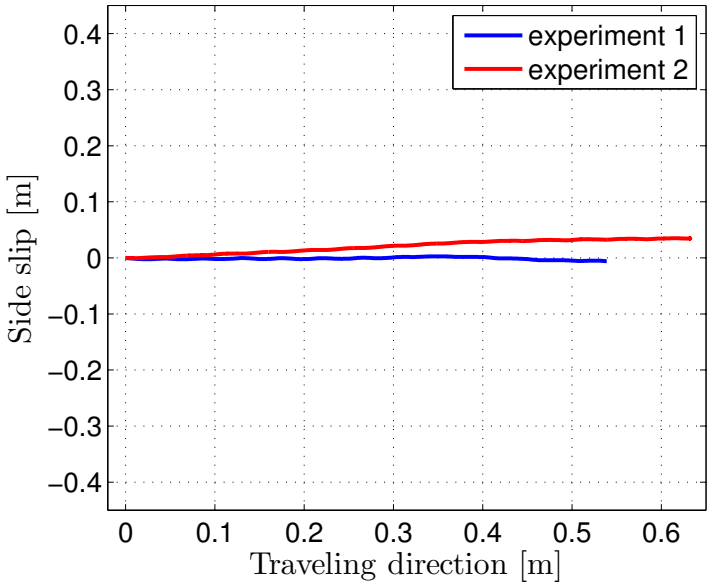

Figure 59: Velocity dependance

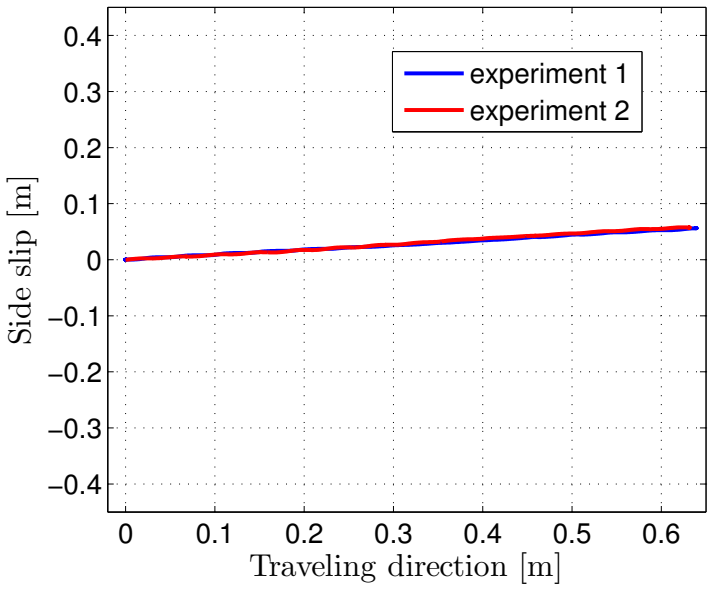

Figure 60: Velocity dependance

used to send the commands to the rover and a *Leica Viva TS15*: a total station used that, thanks to a prism mounted on the rover, can track and record its movements (Figure 61). The goal of this test is to show the importance of a correct evaluation of the soil parameters. Using a correct model, with the wrong parameters, leads to a complete misleading result as shown in Figure 62. For this reason lunar regolith replica is used to prepare the model for the Lunar mission and usually the model based approach, like the one presented in this thesis,

Figure 61: Sendai beach field test

is used in couples with sensor based approach, that computes real time the inputs, based on the odometry data.

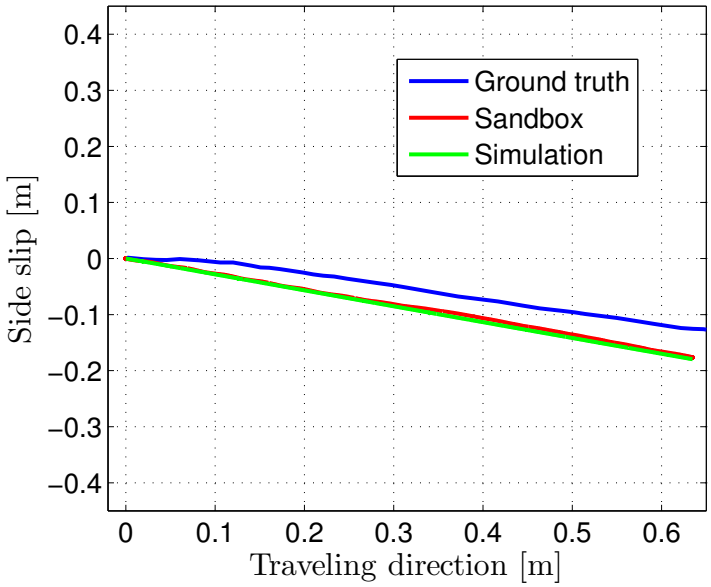

Figure 62: Results comparison with the field test

4.3 SIDE SLIP COMPENSATION

To traverse a slope without slipping, various strategies can be adopted that can usually be divided in discrete control or continuous con-

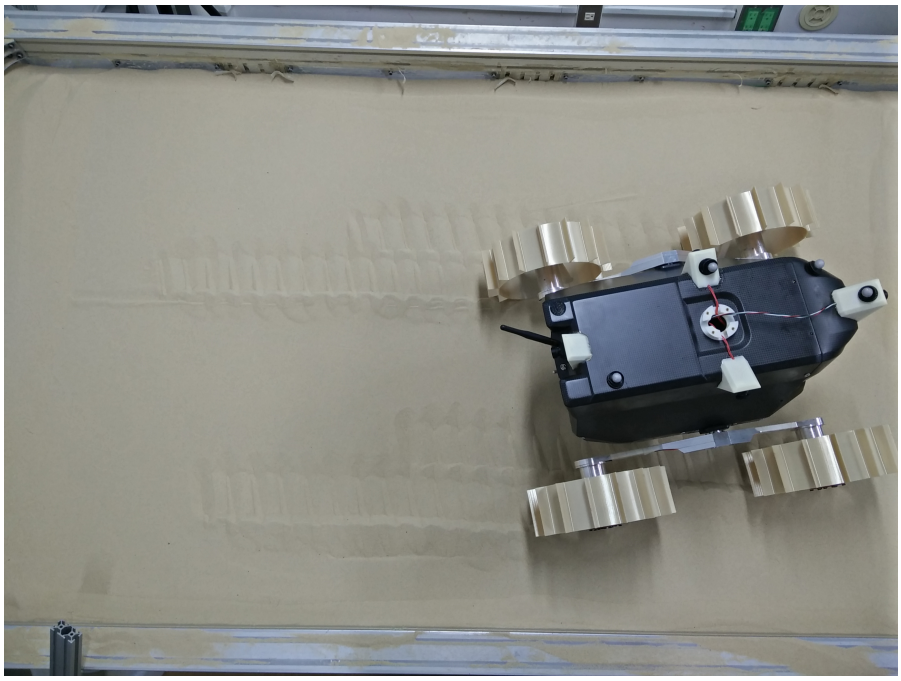

Figure 63: Ideal result

trol. The first considers only spot turns and straight movements. The second uses different types of steering maneuvering. Nagaoka et al. [15] verified that performing spot turns and consequently moving in straight lines, is energetically more efficient than steering. Moreover, this strategy fits the mobility features of Moonraker.
The proposed strategy consist in knowing a priori the correct attitude to assume to traverse horizontally the slope, avoiding the skidding. It is possible analyzing a "slope-attitude" correlation. Having a constant slope, through an iterative procedure, it is possible to define the initial angle γ_0 that causes the rover to move along the x_h axis.
The first step for this procedure is performing a simulation with the rover facing the arrival point. In the code this is traduced with the angle γ_0 equal to zero. As previously shown this will produce a linear motion, characterized by a constant slip angle β. The value of β is used in the second iteration as initial guess for γ_0. In the following iterations it is possible to adjust the attitude angle, using the desired convergence method, and checking to the value of the lateral velocity in the horizon reference frame v_{yh}, until the desired precision is reached.
This technique is used for the two cases under analysis. To make easier the testing and the usable the result, the solving angle is stopped at the closest integer number, that result to be 15° and 7° respectively for the 20° and 10° slope angle. Figure 64 and 65 present the found solution. In the first case the dynamic is well simulated and the result is close to the aimed one, and the track of the wheels is shown in Figure 63. The 10° case presents a higher error, that can be related to

the lower simulation precision obtained in the tuning. The solution errors are summed in Table (5), where are reported in the first line the errors relative to the difference between the simulation and the test, and in the second line the error of the test with respect to the zero skidding. In this case, as for the tuning procedure, the effect of the focus on the 20° slope case is evident.

Performing this analysis for different values of the slope angle α,

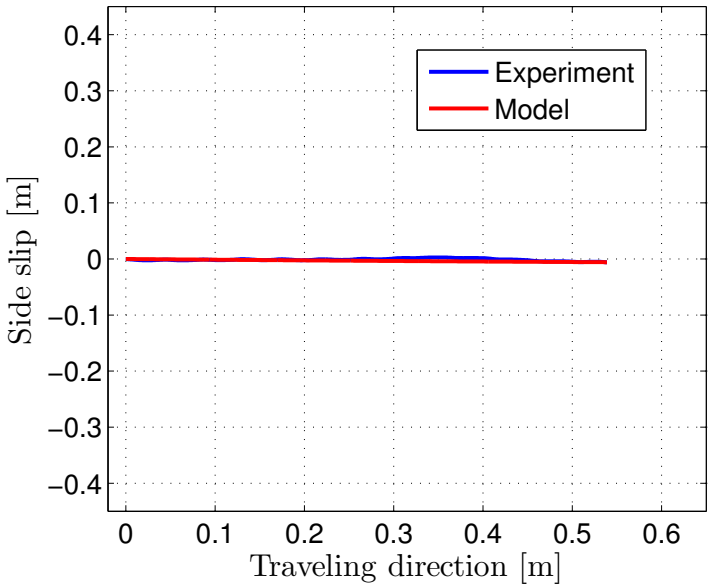

Figure 64: Side slip compensation

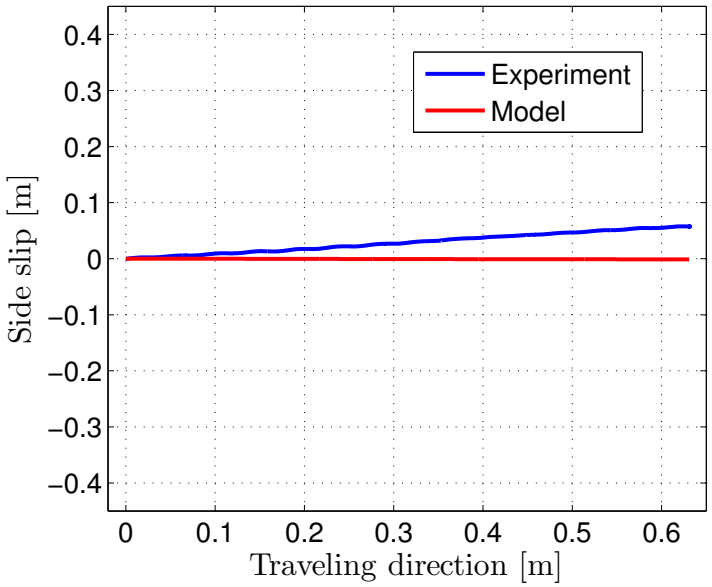

Figure 65: Side slip compensation

	10°slope	20°slope
Simulation error	9.27%	0.04%
Solution error	9.09%	1.07%

Table 5: Solution errors

it is possible to create a mapping of the initial attitude to assume to correctly traverse. The solutions are computed for sloped equal to 0°, 5°, 10°, 15° and 20°. The obtained results are interpolated, and the curve is plotted in Figure 66.

The flowchart (67) summarize the procedure to evaluate the correct

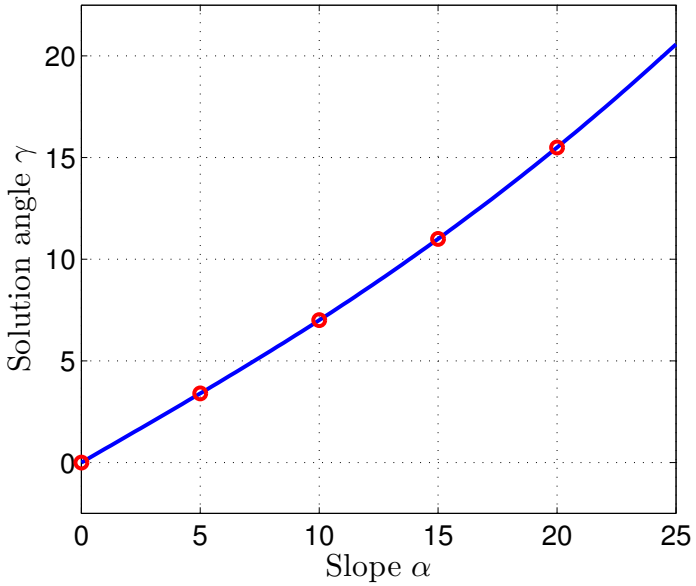

Figure 66: Slope-attitude correlation

initial attitude.

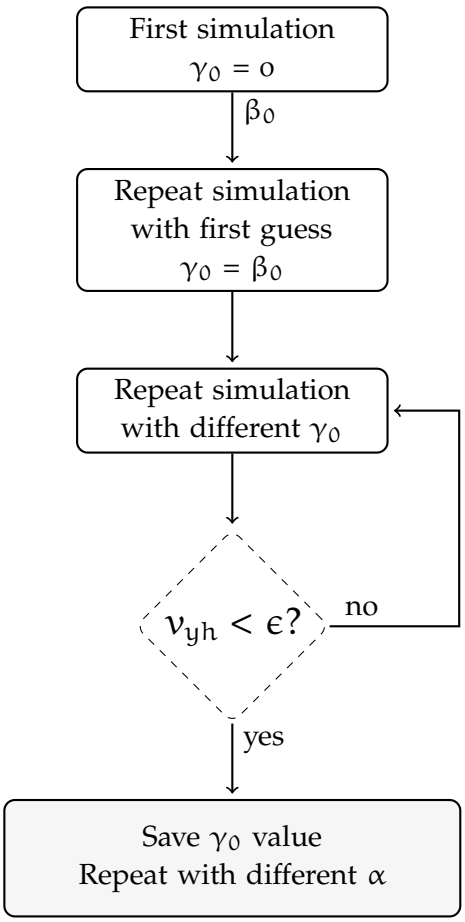

Figure 67: Numerical simulation flowchart

5

CONCLUSIONS

By the end of 2017, team HAKUTO will send a rover to the Moon, in the attempt to win the Google Lunar XPRIZE. The competing teams are asked to land a rover on the Moon and perform some operations that includes the maneuvering. One of the aspects that makes it troublesome, is the sandy and sloped nature of the Lunar terrain. Due to the loose soil, a certain slippage is present and, if not considered, can lead failures or loss of the mission. The slippage affects the motion both on the longitudinal direction and in the lateral direction. On the longitudinal, it causes a mismatch of the traveled distance and could cause the rover to dig and get stuck in the soil. The lateral slip (or skid) causes, when moving on an inclined terrain, an undesired lateral velocity. To deal with the second, an approach based on the on board sensors is used along with a model that simulates the described dynamics. This kind of model is analyzed in this thesis.
Firstly the mathematics, used to characterize the interaction between the soil and the wheels, is described. Two proposed models are compared to the results obtained through tests performed on a single wheel, having a force/torque sensor mounted on it.
A Simulink® model is used to simulate the dynamic behaviour of the rover. Being the force model computational demanding, a possible method to overcome this problem is proposed. The possibility of having as input the torque applied to the wheels or the wheel velocity itself is discussed. The later is preferred because it better represent the test setup, being the wheel velocity the input variable used in the tests. A test campaign is performed to compare the obtained simulator with the ground truth, focusing on slope of 10° and 20°. This tests are also used to demonstrate the uncorrelation of the wheel velocity with the resulting forces and trajectory. Being the aim of the thesis to properly simulate the motion of a specific type of rover, a tuning is computed, varying only one parameter in the force model and one parameter in the dynamic model, and focusing on the 20° slope case. Not being the optimal solution, good results are obtained on the studied case, less accurate for the other considered case.
Having the tuned model, an approach to compensate the side slip is described: the proper angle with respect to the traverse direction is evaluated through an iterative procedure. The proposed solution is tested and its accuracy evaluated.
This thesis is the first part of an ongoing research to deal with this aspect of the mission. Further tests are being performed on both the force determination and dynamic simulation, along with spot turn si-

mulations are also being developed. Particular attention must be put in the extremely precise placement of the rover for the tests in the sandbox. Minor imprecisions in the initial attitude lead to important errors of the results. In this thesis is shown the importance of a precise determination of the soil parameters, that can dramatically affect the movements. The study of a proper way to tune the multi-parameters model is also mandatory.

BIBLIOGRAPHY

[1] M. G. Bekker, *Off-The-Road Locomotion*, Ann Arbor, MI, USA, The University of Michigan Press, 1960

[2] M. G. Bekker, *Introduction to Terrain-Vehicle Systems*, Ann Arbor, MI, USA, The University of Michigan Press, 1969

[3] J. Y. Wong, *Theory of Ground Vehicles*, 4th ed. Hoboken, New Jersey: John Wiley & Sons, Inc., 2008

[4] S. Higa, K. Sawada, K. Nagaoka, K. Nagatani, K. Yoshida, *Measurement of Stress Distributions of a Wheel with Grousers Traveling on Loose Soil*, Proceedings of 2016 IEEE International Conference on Robotics and Automation (ICRA) Stockholm, Sweden, May 16-21, 2016

[5] K. Yoshida, G. Ishigami, *Steering Characteristics of a Rigid Wheel for Exploration on Loose Soil*, Proceedings of 2004 IEEElRSJ International Conference on lntelllgent Robots and Systems September 28 - October 2,2004, Sendal, Japan

[6] G. Ishigami, *Terramechanics-based Analysis and Control for Lunar/Planetary Exploration Robots*, PhD thesis, Tohoku University, 2008

[7] G. Ishigami, A. Miwa, K. Nagatani, K. Yoshida, *Terramechanics-based model for steering maneuver of planetary exploration rovers on loose soil*, Journal of Field Robotics, 24:233–250, 2007

[8] G. Ishigami, K. Nagatani, K. Yoshida, *Slope traversal experiments with slip compensation control for lunar/planetary exploration rover*, Proceedings of the 2008 IEEE Int. Conf. on Robotics and Automation (ICRA2008), pages 2295–2300, Pasadena, CA

[9] G. Ishigami, K. Nagatani, K. Yoshida, *Trafficability analysis for lunar/ planetary exploration rover using thrust-cornering characteristic diagram*, Proceedings of the 2008 IEEE Int. Conf. on Intelligent Robots and Systems (IROS2008), pages 2228–2233, Nice, France

[10] G. Ishigami, K. Nagatani, K. Yoshida *Path following control with slip compensation on loose soil for exploration rover*, 2006 IEEE/RSJ International Conference on Intelligent Robots and Systems. IEEE, 2006

[11] M. Sutoh, *Traveling Performance Analysis of Lunar/Planetary Robots on Loose Soil*, PhD thesis, Tohoku University, 2013

[12] M. Sutoh, K. Nagatani, K. Yoshida, *Evaluation of influence of surface shape of wheel on traveling performance of planetary rover over slope*, Proceedings of the 17th International Conference of International Society for Terrain-Vehicle Systems, Blacksburg, VA, USA, September 2011

[13] M. Sutoh, K. Nagaoka, K. Nagatani, K. Yoshida, *Evaluation of influence of wheel surface shapes on tractive efficiencies of planetary rovers in various soil environments*, Proceedings of the 11th International Symposium on

Artificial Intelligence, Robotics and Automation in Space, Turin, Italy, September 2012, pp. 7c–3

[14] Z. Janosi and B. Hanamoto, *The analytical determination of drawbar pull as a function of slip for tracked vehicle*, Proceedings of the 1st Int. Conf. on Terrain-Vehicle Systems, Torio, 1961

[15] K. Nagaoka, K. Nakata, S. Higa, K. Yoshida, *Mobility Characteristics and Control of a Skid-Steering Micro-Rover for Planetary Exploration on Loose Soil*, Proceedings of the 13th International Symposium on Artificial Intelligence, Robotics and Automation in Space, #S-9a-4, 2016

[16] N. Britton, J. Walker, K. Yoshida, T. Shimuzu, T. Paniccia, K. Nakata, *Four-Wheel Rover Performance Analysis at Lunar Analog Test*, Field and Service Robotics. Springer International Publishing, 2016

[17] Walker, John, et al. *Update on the Qualification of the Hakuto Micro-rover for the Google Lunar X-Prize*, Field and Service Robotics. Springer International Publishing, 2016

[18] L. Ojeda, D. Cruz, G. Reina, J. Borenstein, *Current-based slippage detection and odometry correction for mobile robots and planetary rovers*, IEEE Transactions on Robotics 22.2 (2006): 366-378

[19] T. Kanoui, H.i Fujimoto, *Slip-ratio based yaw-rate control with driving stiffness identification for electric vehicle*, Proceedings of 9th International Symposium on Advanced Vehicle Control. 2008

[20] F. Solc, J. Sembera, *Kinetic model of a skid steered robot*, Proceedings of the 7th WSEAS Interna-tional Conference on Signal Processing, Robotics and Automation. Cambridge, UK. 2008

[21] K. Fujii, H. Fujimoto, *Traction control based on slip ratio estimation without detecting vehicle speed for electric vehicle*, Fourth Power Conversion Conference-NAGOYA. 2007

[22] K. Kozłowski, D. Pazderski *Modeling and control of a 4-wheel skid-steering mobile robot*, Int. J. Appl. Math. Comput. Sci 14.4 (2004): 477-496

[23] H. Inotsume, K. Skonieczny, D. S. Wettergreen, *Analysis of Grouser Performance to Develop Guidelines for Design for Planetary Rovers*

[24] G. Ishigami, K. Nagatani, K. Yoshida, *Locomotion Mechanics of Wheeled Rovers on Simulated Lunar Soil*, Proceedings of 17th Workshop on JAXA Astrodynamics and Flight Mechanics. 2008

[25] K. Skonieczny, S. J. Moreland, D. S. Wettergreen, *A grouser spacing equation for determining appropriate geometry of planetary rover wheels*, 2012 IEEE/RSJ International Conference on Intelligent Robots and Systems. IEEE, 2012

[26] K. Yoshida, H. Hamano, T. Watanabe, *Slip-based traction control of a planetary rover*, Experimental Robotics VIII. Springer Berlin Heidelberg, 2003. 644-653

[27] M. Cross, A. Ellery, *Estimating terrain parameters for a rigid wheeled rover using neural networks*, Journal of Terramechanics 50.3 (2013): 165-174

[28] O. Onafeko, A. R. Reece, *Soil stresses and deformations beneath rigid wheels*, Journal of Terramechanics 4.1 (1967): 59-80

[29] J. Y. Wong, A. R. Reece, *Prediction of rigid wheel performance based on the analysis of soil-wheel stresses part I. Performance of driven rigid wheels*, Journal of Terramechanics 4.1 (1967): 81-98

[30] K. Iagnemma, et al., *Terramechanics modeling of Mars surface exploration rovers for simulation and parameter estimation*, ASME 2011 International Design Engineering Technical Conferences and Computers and Information in Engineering Conference. American Society of Mechanical Engineers, 2011

[31] K. Yoshida, T. Shiwa, M. Oda, *Dynamic simulation of an articulated off-road vehicle*, AIAA Modeling & Simulation Technologies Conf. Paper. 1998

[32] http://www.nasa.gov/50th/50th_magazine/lunarExploration.html

[33] http://lunar.xprize.org/

[34] http://team-hakuto.jp/en/

[35] http://ispace-inc.com/